

Multiple Model Control for Teleoperation
Under Time Delay

MULTIPLE MODEL CONTROL FOR TELEOPERATION UNDER
TIME DELAY

BY
ALI SHAHDI, B.Sc.

A THESIS
SUBMITTED TO THE DEPARTMENT OF ELECTRICAL & COMPUTER ENGINEERING
AND THE SCHOOL OF GRADUATE STUDIES
OF MCMASTER UNIVERSITY
IN PARTIAL FULFILMENT OF THE REQUIREMENTS
FOR THE DEGREE OF
MASTER OF APPLIED SCIENCE

© Copyright by Ali Shahdi, September 2005

All Rights Reserved

Master of Applied Science (2005)
(Electrical & Computer Engineering)

McMaster University
Hamilton, Ontario, Canada

TITLE: Multiple Model Control for Teleoperation Under Time
Delay

AUTHOR: Ali Shahdi
B.Sc., (Electrical Engineering)
Sharif University of Technology, Tehran, Iran

SUPERVISOR: Dr. Shahin Sirouspour

NUMBER OF PAGES: xii, 118

To My Parents

Abstract

Performance and stability of bilateral teleoperation control systems are adversely affected by variations in environment dynamics and time delay in communication channel. Prior relevant research in the literature has mainly yielded control algorithms that sacrifice performance in order to guarantee robust stability. In contrast, this thesis proposes methods to deal with these two main problems in order to maintain the stability without compromising performance.

To handle changes in environment dynamics, a multiple model controller for teleoperation is introduced. It is assumed that the dynamics of the environment are governed by a model from a finite set of environment models at any given time with Markov chain switching between these models. The first-order generalized pseudo-Bayesian (GPB1) multi-model estimation technique is used to identify the effective model at each time step given the sensory observations. The control action is a weighted sum of mode-based control laws that are designed for each mode of operation.

The second major problem in teleoperation systems that this thesis deals with is communication channel time delay. The constant time-delay problem is solved using two different methods, i.e. discrete-time and continuous-time predictive type Linear Quadratic Gaussian (LQG) controllers. The treatment of the problem in

the discrete-time domain allows for the development of a finite dimension state-space model that explicitly encompasses the time delay. The robustness of the controller with respect to uncertainty in the system parameters is examined via Nyquist analysis. In continuous-time, a modified state transformation is proposed to obtain delay-free dynamics based on the original dynamics with delayed inputs and outputs. The application of the continuous-time LQG control synthesis to these reduced dynamics yields a control law that guarantees closed-loop stability and performance. Mode-based controllers are designed for each phase of operation, i.e. free motion/soft contact and contact with rigid environments. Performance objectives such as position tracking and tool impedance shaping for free motion/soft contact, as well as position and force tracking for contact with rigid environments are incorporated into the LQG control design framework.

Simulation and experimental results are presented for each of the proposed controllers in various scenarios. These results demonstrate the effectiveness of the proposed methods in providing a stable transparent interface for teleoperation in free motion and in contact with rigid environments.

Acknowledgements

My deepest gratitude and appreciation is due to my supervisor, Dr. Shahin Sirouspour, for his endless support and guidance. I want to thank him for his tremendous effort and encouragement, during all the stages of my M.Sc. program.

Sincere thanks go to my colleagues at Telerobotics, Haptics, and Computational Vision Lab, Peyman Setoodeh, Forough Farshidi and Magyar Foothill for their kind helps and friendship. I am also grateful to my friends for their kindness, friendship and reminding me that there is life beyond school.

Last but not least, I want to thank my parents who always support and encourage me through my life. Their understanding and patience have made it possible to pass all the steps. Without their supports, completion of this thesis would not have been possible.

Contents

Abstract	iv
Acknowledgements	vi
1 Introduction and Problem Statement	1
1.1 Motivation	1
1.2 Problem Statement and Thesis Contributions	3
1.3 Organization of the Thesis	5
1.4 Related Publications	6
2 Literature Review	7
2.1 Dynamic Uncertainty	8
2.1.1 Robust Controllers	8
2.1.2 Adaptive Controllers	9
2.2 Delay in Communication Channel	10
2.2.1 Passivity-Based Controllers	11
2.2.2 Robust Controllers	12
2.2.3 Predictive Controllers	13
2.3 Control of Time-Delay Systems	13

3	Multiple Model Teleoperation Controller	15
3.1	Introduction	15
3.2	Four-Channel Teleoperation Control Architecture	16
3.3	Multiple Model State Estimation and Control for Teleoperation	21
3.4	Simulation Results	25
3.5	Experimental Results	31
4	Discrete-Time LQG Teleoperation Controller	35
4.1	Introduction	35
4.2	LQG Teleoperation Control	36
4.2.1	Free motion/soft contact	39
4.2.2	Rigid contact	46
4.2.3	LQG control design	48
4.3	Simulation Results	53
4.4	Robust Stability Analysis	58
4.4.1	Robustness against mismatch in environment stiffness	59
4.4.2	Robustness against mismatch in arm mass and environment stiffness	60
4.4.3	Robustness against mismatch in arm mass for rigid contact controller	61
4.5	Experimental Results	62
4.5.1	LQG controller with 63ms delay	62
4.5.2	LQG controller with 125ms delay	64
4.5.3	LQG controller with 250ms delay	65
4.5.4	Two-channel controller with 250ms delay	67

5	Continuous-Time LQG Teleoperation Controller	70
5.1	Introduction	70
5.2	Delayed System Reduction and Control	71
5.3	LQG Teleoperation Control	78
5.3.1	Free motion/soft contact	80
5.3.2	Rigid contact	83
5.3.3	LQG control synthesis	87
5.4	Simulation Results	89
5.5	Experimental Results	92
5.5.1	LQG controller with 63ms delay	93
5.5.2	LQG controller with 125ms delay	93
5.5.3	LQG controller with 250ms delay	94
6	Conclusions and Future Work	96
A	Proof of Theorem 5.1	99
A.1	Stabilizability	99
A.2	Detectability	104

List of Figures

1.1	Teleoperation control of a robot.	2
3.1	GPB1 method for two models.	23
3.2	Multiple model state estimation and control for two modes.	24
3.3	Schematic of the single-axis teleoperation system.	25
3.4	Mode transition probabilities	29
3.5	Position and force tracking in simulation: (a), (b) fixed-gain controller (c), (d) multi-model controller.	30
3.6	The experimental setup.	31
3.7	Position and force tracking in experiment: (a),(b),(c) fixed-gain controller (d),(e),(f) adaptive multi-model controller.	32
3.8	Mode probability transitions in experiment.	33
4.1	Teleoperation controller resides at the master side.	39
4.2	The LQG teleoperation control system.	41
4.3	Position and force tracking in simulation for matched parameters: (a) 125ms delay (b) 250ms delay (c) 500ms delay.	56
4.4	Position and force tracking in simulation for mismatched model parameters: (a) 125ms delay (b) 250ms delay (c) 500ms delay.	58

4.5	Robustness of free motion controller w.r.t. mismatch in environment stiffness ($k_e = 0.1$ in design).	59
4.6	Robustness of free motion controller w.r.t. mismatch in arm mass and environment stiffness ($m_h = 0.35$ and $k_e = 0.1$ in design).	60
4.7	Robustness of rigid contact controller w.r.t. mismatch in arm mass ($m_h = 0.35$ in design).	61
4.8	LQG controller with 63ms delay in experiment: (a) position tracking for master/slave/virtual tool; (b) contact transition (c) force tracking.	63
4.9	LQG controller with 125ms delay in experiment: (a) position tracking for master/slave/virtual tool; (b) contact transition (c) force tracking.	65
4.10	LQG controller with 250ms delay in experiment: (a) position tracking for master/slave/virtual tool; (b) contact transition (c) force tracking.	66
4.11	Two-channel position-position controller with 250ms delay in experiment: (a) position tracking; (b) force tracking (c) compared with desired response obtained from virtual tool.	69
5.1	Linear system with (a) delayed control actions and (b) delayed control actions and delayed measurements	72
5.2	The system architecture when teleoperation controller resides at the master side.	89
5.3	Position and force tracking in simulation for matched parameters: (a) 125ms delay (b) 250ms delay (c) 500ms delay.	91

5.4	Position and force tracking in simulation for mismatched model parameters: (a) 125ms delay (b) 250ms delay (c) 500ms delay.	92
5.5	LQG controller with 63ms delay in experiment: (a) position tracking for master/slave/virtual tool; (b) contact transition (c) force tracking.	93
5.6	LQG controller with 125ms delay in experiment: (a) position tracking for master/slave/virtual tool; (b) contact transition (c) force tracking.	94
5.7	LQG controller with 250ms delay in experiment: (a) position tracking for master/slave/virtual tool; (b) contact transition (c) force tracking.	95

Chapter 1

Introduction and Problem Statement

1.1 Motivation

The need of human skill and intelligence in the areas where he/she can not be present has been the basic idea for formation of teleoperation systems. Over the past three decades, the use of teleoperation technology have been steadily growing in a wide range of applications [1–3]. These applications include space operation [4–7], underwater exploration [8, 9], mining [10], nuclear material handling [11], toxic material handling, the entertainment industry, and more recently health care [12, 13].

Telerobotic systems deliver the human intelligence and skills combined with robot precision, repeatability and power to inaccessible and/or remote environments. This is achieved through coordinated control of a master robotic arm, locally used by the operator, and a slave manipulator which mimics the operator's actions in the task environment.

Five distinct elements constitute a bilateral teleoperation system as shown in

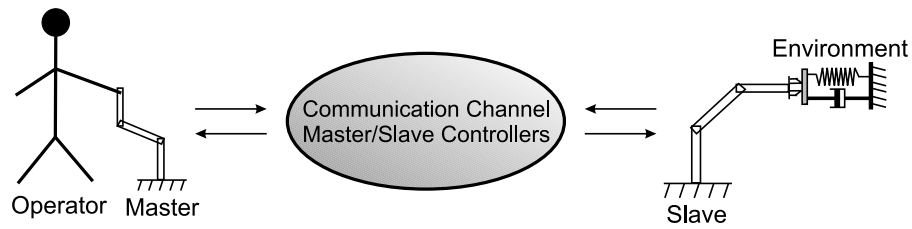


Figure 1.1: Teleoperation control of a robot.

Figure 1.1. These are the human operator, master robot, controllers and communication channel, slave robot, and the environment [14]. The human operator uses the master device to interact with the task environment through the slave robot. The operation is coordinated via the teleoperation and local controllers.

Unilateral teleoperators transmit position and/or force commands to the slave site and relay visual sensory information from the task back to the master site. In this context, the operator is an intelligent controller that utilizes the sensory feedback to control the slave arm and perform the task. Bilateral teleoperators provide the operator with additional information such as kinesthetic and haptic feedback through the master device. Their goal is to facilitate task execution through the establishment of virtual presence in the task environment, a performance objective often referred to as ideal transparency in the literature [15]. Teleoperation control design involves a trade-off between the often conflicting requirements of stability and performance [15]. The next section will discuss the problems involved in teleoperation systems and the proposed solutions.

1.2 Problem Statement and Thesis Contributions

- **Problem 1** Operation in remote environments often involves changes in the environment parameters, i.e. free motion, contact with a soft or rigid environment. Using a fixed controller for all the operation modes can make the design too conservative, which can sacrifice either stability or performance in order to achieve the other.
- **Problem 2** Depending on the medium of communication in a teleoperation application, the data exchange between the master and slave sites may suffer from constant or time-varying latency. Such delay can not only degrade the performance of telerobotic systems but also cause instability. The time delay at which a teleoperation system would become unstable depends on factors such as master and slave dynamics, controller architecture and bandwidth, as well as the environment and operator dynamics. Unilateral teleoperators are less sensitive to delay since their feedback loop is closed only through the human's visual perception and motor control system with a relatively small bandwidth. In contrast, bilateral teleoperators entail high bandwidth feedback loops that provide kinesthetic coupling and force tracking between the master and slave. This makes them prone to instability due to the communication delay. Several controllers have been proposed in the literature to deal with the delay problem, which will be pointed in the next chapter. Nevertheless, a major disadvantage of such methods is that their robust stability is gained by sacrificing the transparency.

The following solutions are presented in this thesis to solve the stated problems.

- **Solution to Problem 1** Adaptive controllers can avoid the trade-off between stability and performance by changing their parameters and/or structure in response to variations in system dynamics. Many adaptive controllers have been developed for teleoperation systems, which will be addressed in the next chapter. Unfortunately, parameter convergence in adaptive controllers is often sensitive to modelling errors and the estimated parameters must be bounded to avoid instability due to parameter divergence. Also, most adaptive teleoperation methods assume a fixed control structure and only adjust their parameters. However, a change in control structure can be beneficial for teleoperation if the nature of environment varies drastically. In this work a multiple-model estimation and control scheme for teleoperation in unknown environments is introduced. This method is addressed in full detail in Chapter 3.
- **Solution to Problem 2** Bilateral teleoperation controllers based on Linear Quadratic Gaussian control [16] are introduced to deal with delay problem. In the discrete-time domain, this is motivated by the fact that time delay can be modelled by finite dimension states in the discrete time. In our approach, the latency is assumed to be *a priori* known constant. Unknown variable delays can be estimated and made constant through synchronization and buffering [17, 18]. The discrete-time LQG controller is described in chapter 4.

One drawback of this approach is that the number of states is proportional to the delay and the control rate. Therefore to reduce the computational load and avoid potential numerical problems, the sampling rate must be limited

as the delay increases. This may not be desirable since a low sampling rate can negatively impact the closed-loop response. Hence, to solve this problem, a novel reduction technique for multi-input/multi-output (MIMO) control systems with non-identical delays in measurement and control signals is introduced and utilized to produce a delay-free variation of the teleoperation system dynamics. An LQG observer/controller is synthesized to achieve transparency objectives using position and force measurements at the master and slave sides. The details of this method are presented in Chapter 5.

The teleoperation control formulation as an LQG optimal control design allows for the systematic optimization of the transparency measures while maintaining stability. The performance indices used include non-delayed position tracking, force tracking, and virtual tool impedance shaping.

1.3 Organization of the Thesis

The thesis is organized as follows. Telerobotic literature has been reviewed in Chapter 2, with more emphasis on the stated problems. Multiple model controller for teleoperation is presented in Chapter 3. Chapters 4 and 5 address the delay problem, where in Chapter 4, discrete-time LQG method is introduced and in Chapter 5, continuous-time LQG controller is addressed. Simulation and experimental results in various scenarios are given for each of these three methods in their corresponding chapters. The thesis is concluded in Chapter 7.

1.4 Related Publications

- A. Shahdi and S. Sirouspour, "Multiple Model Control for Teleoperation in Unknown Environments", in Proc. IEEE International Conference on Robotics and Automation, April 2005, Barcelona, Spain, pp. 715-720.
- S. Sirouspour and A. Shahdi, "Bilateral Teleoperation under Communication Time Delay Using an LQG Optimal Controller", in Proc. IEEE International Conference on Control Applications. August 2005, Toronto, Canada, pp. 1257-1262.
- S. Sirouspour and A. Shahdi, "LQG Controller Design for Teleoperation under Communication Time Delay", Submitted to the International Journal of Robotics Research (revised).
- S. Sirouspour and A. Shahdi, "Model Predictive Transparent Teleoperation under Communication Time Delay", Submitted to the IEEE transaction of Robotics and Automation.
- A. Shahdi and S. Sirouspour, "Multi-model Control Synthesis for Transparent Teleoperation under Constant Time Delay", Submitted to 2006 IEEE International Conference on Robotics and Automation.

Chapter 2

Literature Review

Robotics literature proposes several control architectures for teleoperation that employ bidirectional flow of force and position information between master and slave. These include position-position [19], position-force [20,21], force-force [22], and the four-channel [15,23] teleoperation approaches. Linear circuit theory has been used to design and analyze teleoperation controllers. Hannaford [20] proposed a bilateral impedance control architecture using well-known hybrid two-port models from circuit theory. The two-port model of a teleoperation system can be obtained by measuring input-output characteristics of this two-port network. Hashtrudi-zaad and Salcudean [24] gave a comprehensive review of the applications of the circuit theory in modelling and design of controllers for teleoperation systems. In this article, controller design for impedance modelled teleoperation systems is extended to four-channel bilateral teleoperators with either impedance or admittance models. Also, the set of control parameters that provide the systems with ideal transparency are calculated for each type of teleoperation. The next two sections will review the literature concerning two main problems in teleoperation, i.e.

dynamics uncertainties and delay in communication channel.

2.1 Dynamic Uncertainty

Extensive amount of research have been done to cope with the problem of dynamics uncertainty in teleoperation systems. These uncertainties include hand and environment parameters as well as master and slave characteristics. The following sections provide a categorized overview of the proposed controllers dealing with the dynamic uncertainty problem.

2.1.1 Robust Controllers

Robust controllers have been widely used in control of robotic manipulators [25–29]. Linear controllers based on the μ -synthesis and H_∞ theories have been developed to achieve robust stability and transparency in the presence of uncertainties in the system dynamics. Colgate [30] introduced an impedance shaping control technique for teleoperation systems. A general condition for the robustness of a bilateral teleoperator is calculated using the structured singular value(μ). Kazerooni et. al. [22] proposed a control method based on H_∞ -optimal control for force-force teleoperation systems. Hu et. al. [31] formulated the controller design parameter as a multiple objective optimization problem and incorporated robust stability into the design of the controller. Recently, Sirouspour [32] proposed a robust controller for multi-master/multi-slave cooperative teleoperation based on μ -synthesis. Ryu et al. [33] have proposed an energy-based method for stable teleoperation using

time-domain passivity control under no communication delay. Recently, a time-domain passivity-based controller has been proposed for teleoperation under a wide variety of environments and operating speeds in the absence of time delay [34].

These approaches can lead to conservative designs if variations (uncertainty) in the system dynamics are large as it is often the case in teleoperation. This is due to the fixed structure and/or parameters of the controller.

2.1.2 Adaptive Controllers

Varying controller parameters and/or structure helps adaptive controller to avoid the trade-off between system's performance and stability. Kress and Jansen [35] have introduced an automatic tuning technique that can determine the gain settings automatically with an intelligent search technique. Hashtrudi-zaad and Salcudean [36] have proposed a class of indirect adaptive bilateral control schemes. Their method uses measurements of master and slave position, velocity and acceleration to estimate the environment impedance. Shi et. al. [37] have introduced new transparency concepts suitable for adaptive control of teleoperation systems with time varying parameters. Zhu and Salcudean [38] have proposed nonlinear adaptive motion/force control for stable teleoperation. Some other adaptive teleoperation control schemes can be found in [39,40]. Most adaptive teleoperation methods use a fixed control structure. However, control structure can be changed to deal with the variation of environment dynamics.

In this thesis a multiple-model adaptive controller is used for teleoperation in

unknown environments. Multiple-model controllers assume that system dynamics obey a model from a given finite set of models (with known or unknown parameters). These methods have previously been used for control of robot manipulators. Ciliz and Narendra [41] utilized multiple models of a manipulator for identifying its unknown inertial parameters as well as the parameters of its load. Leaby and Sablan [42] augmented a mode-based controller with multiple-model adaptive estimation to minimize position trajectory tracking errors. Narendra and Balakrishnan [43] presented a general methodology for adaptive control using multiple models, switching and tuning. They proposed specific performance indexes in terms of model outputs and how to choose the best model using these indices. Zhang and Jiang [44] adopted interacting multiple model (IMM) filters to develop an active fault tolerant controller.

2.2 Delay in Communication Channel

This section focuses on the part of the literature dealing with the second major problem of teleoperation, i.e. delay in data transmission. The delay can be anywhere from few milliseconds to several minutes. Such amount of delay can degrade the system's performance as well as causing instability problems. Teleoperation control design embodies a trade-off between the often conflicting requirements of stability and performance. Unfortunately, the potential for instability increases by the level of the performance of the controller. In [45], a rigorous analysis of the robust stability of bilateral teleoperation with respect to time delay is presented. In [46], some existing teleoperation control schemes that address the issue of time latency are compared from the stability and performance perspectives. Lee

and Lee [47] have proposed modelling and design of a teleoperator control system for time delays of up to a few seconds. Desired performance and robustness are achieved under shared compliance control. Also, the concept of telemonitoring force feedback for teleoperation under short time delays is introduced. In [48] a quantitative evaluation of operability has investigated that depends on communication time delay. Mirfakhrai and Payandeh [49] have developed a stochastic model for time delay over internet, which is becoming more popular as a communication medium. Dynamic analysis of a teleoperation system with time delay is presented in [50] where state convergence is used. Imaida et. al. [51] have shown that, by proving sufficient damping at the master and slave ends, a delayed bilateral position-position teleoperation system can be stabilized, though at the expense of a sluggish response. The rest of this section gives a categorized review of the literature coping with time delay problem.

2.2.1 Passivity-Based Controllers

The scattering theory and the concept of passivity have been employed to guarantee stable teleoperation irrespective of the amount of time delay [52–55]. Niemeyer and Slotine [53] used the idea of passivity to provide energy conservation and to guarantee system's stability. Yokokohji et al. [56] have introduced an energy monitoring method to achieve passivity. In [57], an adaptation of the line terminating impedance functions is proposed to remedy the loss of transparency in bilateral

teleoperation based on the scattering theory. Wave variables are used to characterize systems with time delay which resulted in a stable force-reflecting teleoperation scheme. Nevertheless, a major disadvantage of such methods is that their robust stability is gained by sacrificing the transparency. A survey on wave-variable based controllers for teleoperation can be found in [58]. Yokokohji et. al. [59] proposed a control scheme based on wave variables, which minimize the performance degradation in spite of time delay fluctuations. Benedetti et. al. [60] introduced a force-feedback teleoperation controller based on wave-variables for variable time delays. In [61] a wave-variable based controller is developed which can match the system parameters with changes in the delay by predicting the future values of delay. Ueda and Yoshikawa [62] presented a force-reflecting teleoperation controller with time delay using wave transmission methods. Conditions of stability, for the proposed controller are derived.

2.2.2 Robust Controllers

Leung et. al. [21] introduce a method based on μ -synthesis and H_∞ control to design a controller for teleoperation with a known delay. Yan and Salcudean [63] proposed a controller design method based on H_∞ theory. The goal of the design is to find a stable controller with optimal performance for teleoperation under communication time delay.

2.2.3 Predictive Controllers

Predictive control methods such as the Smith Predictor have also been developed for teleoperation [46, 64]. In [64], the wave-based teleoperation controller is combined with a Smith Predictor, a Kalman Filter, and an energy regulator to improve the performance. Ganjefar et. al. [65] have discussed the behavior of Smith Predictor in teleoperation systems with respect to modelling and time delay errors. In [66] predictive model-based controller is proposed for teleoperation with time-delay using state prediction. Different predictive force-feedback methods are also presented. References [67] and [68] have proposed predictive controller techniques for teleoperation with unbounded delays. Prokopiou et. al. [69] have proposed a predictive controller for teleoperators based on prediction of human hand position and force. Polynomial or spline predictor have been used to predict master's state. The method has shown a good performance in short time delays and for smooth hand movements. Other techniques such as predictive displays and virtual environments rely on accurate models of the task environment to provide the operator with a realistic delay-free simulated response of the remote manipulator and environment [4, 70–72].

2.3 Control of Time-Delay Systems

There has been considerable effort in the stability analysis and control synthesis for the time-delayed systems and interested reader is referred to the following survey papers on this topic [73–75]. Robust stability analysis of systems with time delay can be found in these survey papers [76, 77]. In particular, Kwon et al. [78] and

later Artstein [79] introduced a transformation to reduce an infinite-dimensional continuous-time linear control system with delayed control actions to an equivalent control system without delay. However, this transformation is not suitable for teleoperation systems where both measurements and control actions are delayed. Therefore, a modified version of the transformation is introduced and utilized in chapter 5.

Chapter 3

Multiple Model Teleoperation Controller

3.1 Introduction

In this chapter the problem of environment uncertainty in teleoperation is considered. To deal with this problem a multiple-model estimation and control scheme for teleoperation is proposed. The dynamics of the environment are assumed to be among a set of models. Mode-based Kalman filters which run in parallel predict the sensor measurements. Prediction errors are used to calculate the probability of each model being the correct model. Mode-based controllers' outputs and the calculated probabilities are used to build the control signal.

This chapter is organized as follows. Section 3.2 introduces the four-channel teleoperation architecture. Section 3.3 proposes the multi-model estimation and control. The results of numerical simulations and experimental results are discussed in sections 3.4 and 3.5.

3.2 Four-Channel Teleoperation Control Architecture

The haptic interfaces employed in teleoperation are generally rigid multi-body mechanical devices with second-order nonlinear dynamics requiring nonlinear modelling, analysis and control design. However, such dynamics can be rendered linear through the application of local dynamic linearization control laws [80]. We further assume that the linearized dynamics are decoupled in different axes of motion. It should be noted that during contact, a coupling among the axes may exist due to the presence of a tangential friction force that is proportional to the normal force. However if the contact along the normal axis is stable, the normal force and hence the tangential friction force are bounded and can be treated as disturbance to the motion in the tangential axis. Such disturbances can be handled by the controllers that will be introduced later. Considering the above assumptions, we only treat a single-axis problem, though our approach can be extended to the multi-axis case.

The linearized dynamics of the master device are governed by

$$m_m \ddot{x}_m + b_m \dot{x}_m + k_m x_m = f_{cm} + f_h \quad (3.1)$$

where m_m , b_m , and k_m are mass, damping, and stiffness of the master interface, and x_m is its position; f_{cm} is the control signal and f_h is the operator/device interaction force. The operator's arm dynamics are approximated by a second-order linear time-invariant differential equation

$$m_h \ddot{x}_m + b_h \dot{x}_m + k_h x_m = f_h^* - f_h \quad (3.2)$$

where m_h , b_h , and k_h are mass, damping and stiffness of the operator's arm, respectively; x_m has been defined in (3.1); f_h^* is the operator's intentional force and is modelled as an exogenous input to the system. This is in addition to the arm's dynamic reaction force which is a function of the master motion variables. In general, dynamics of the arm are nonlinear, time-dependent, and posture-dependent. However, linear models have been successfully employed by previous researchers in their work [38,81] and are adopted here as well. The arm dynamics in (3.2) can be incorporated into the master dynamics in (3.1) as follows

$$(m_m + m_h)\ddot{x}_m + (b_m + b_h)\dot{x}_m + (k_m + k_h)x_m = f_{cm} + f_h^* \quad (3.3)$$

The combined master and arm linearized dynamics can be written in the form of state space equations, i.e.

$$\begin{bmatrix} \dot{x}_m \\ \ddot{x}_m \end{bmatrix} = \begin{bmatrix} 0 & 1 \\ -\frac{k_m+k_h}{m_m+m_h} & -\frac{b_m+b_h}{m_m+m_h} \end{bmatrix} \begin{bmatrix} x_m \\ \dot{x}_m \end{bmatrix} + \begin{bmatrix} 0 & 0 \\ \frac{1}{m_m+m_h} & \frac{1}{m_m+m_h} \end{bmatrix} \begin{bmatrix} f_{cm} \\ f_h^* \end{bmatrix} \quad (3.4)$$

$$\begin{bmatrix} x_m \\ f_h \end{bmatrix} = \begin{bmatrix} 1 & 0 \\ \frac{m_h(k_m+k_h)}{m_m+m_h} - k_h & \frac{m_h(b_m+b_h)}{m_m+m_h} - b_h \end{bmatrix} \begin{bmatrix} x_m \\ \dot{x}_m \end{bmatrix} + \begin{bmatrix} 0 & 0 \\ -\frac{m_h}{m_m+m_h} & 1 - \frac{m_h}{m_m+m_h} \end{bmatrix} \begin{bmatrix} f_{cm} \\ f_h^* \end{bmatrix} \quad (3.5)$$

The dynamics of the slave robot are similar to those of the master robot, i.e.

second-order and nonlinear. The application of a local dynamic feedback linearizing control law produces the following linear dynamics

$$m_s \ddot{x}_s + b_s \dot{x}_s + k_s x_s = f_{cs} - f_e \quad (3.6)$$

where x_s is the position of the slave; m_s , b_s , and k_s are the slave mass, damping, and stiffness, respectively; f_{cs} is the control signal and f_e is the environment reaction force. The reaction force for compliant environments can be modelled by

$$f_e = \begin{cases} m_e \ddot{x}_s + b_e \dot{x}_s + k_e x_s + f_e^* & \text{in contact} \\ 0 & \text{free motion} \end{cases} \quad (3.7)$$

and f_e^* is the exogenous environment force. This can be combined with the slave dynamics in (3.6) to obtain

$$(m_s + \sigma_f m_e) \ddot{x}_s + (b_s + \sigma_f b_e) \dot{x}_s + (k_s + \sigma_f k_e) x_s = f_{cs} - \sigma_f f_e^* \quad (3.8)$$

where

$$\sigma_f = \begin{cases} 1 & \text{slave in contact} \\ 0 & \text{slave in free motion} \end{cases} \quad (3.9)$$

The state space equivalents of the above dynamics are given by

$$\begin{bmatrix} \dot{x}_s \\ \ddot{x}_s \end{bmatrix} = \begin{bmatrix} 0 & 1 \\ -\frac{k_s + \sigma_f k_e}{m_s + \sigma_f m_e} & -\frac{b_s + \sigma_f b_e}{m_s + \sigma_f m_e} \end{bmatrix} \begin{bmatrix} x_s \\ \dot{x}_s \end{bmatrix} + \begin{bmatrix} 0 & 0 \\ \frac{1}{m_s + \sigma_f m_e} & \frac{-\sigma_f}{m_s + \sigma_f m_e} \end{bmatrix} \begin{bmatrix} f_{cs} \\ f_e^* \end{bmatrix} \quad (3.10)$$

$$\begin{bmatrix} x_s \\ f_e \end{bmatrix} = \begin{bmatrix} 1 & 0 \\ \frac{\sigma_f m_e (k_s + k_e)}{m_s + m_e} - \sigma_f k_e & \frac{\sigma_f m_e (b_s + b_e)}{m_s + m_e} - \sigma_f b_e \end{bmatrix} \begin{bmatrix} x_m \\ \dot{x}_m \end{bmatrix} + \begin{bmatrix} 0 & 0 \\ -\frac{\sigma_f m_e}{m_s + \sigma_f m_e} & -\sigma_f \left(1 - \frac{m_e}{m_s + m_e}\right) \end{bmatrix} \begin{bmatrix} f_{cs} \\ f_e^* \end{bmatrix} \quad (3.11)$$

Contact with a rigid environment can be modelled as

$$m_s(1 - \sigma_r)\ddot{x}_s + b_s(1 - \sigma_r)\dot{x}_s + k_s(1 - \sigma_r)x_s = f_{cs} - \sigma_r f_e \quad (3.12)$$

and

$$\dot{x}_s = (1 - \sigma_r)\dot{x}_s \quad (3.13)$$

$$\ddot{x}_s = (1 - \sigma_r)\ddot{x}_s \quad (3.14)$$

with σ_r is similarly defined as in (3.9). Therefore during a rigid contact, the slave acceleration and velocity are zero and the environment force is equal to the slave control action. The slave and environment linearized dynamics in case of contact

with rigid environment can be written in the form of state space equations as follows

$$\begin{bmatrix} \dot{x}_s \\ \ddot{x}_s \end{bmatrix} = \begin{bmatrix} 0 & 1 - \sigma_r \\ -(1 - \sigma_r)\frac{k_s}{m_s} & -(1 - \sigma_r)\frac{b_s}{m_s} \end{bmatrix} \begin{bmatrix} x_s \\ \dot{x}_s \end{bmatrix} + \begin{bmatrix} 0 & 0 \\ \frac{1 - \sigma_r}{m_s} & 0 \end{bmatrix} \begin{bmatrix} f_{cs} \\ f_e^* \end{bmatrix} \quad (3.15)$$

$$\begin{bmatrix} x_s \\ f_e \end{bmatrix} = \begin{bmatrix} 1 & 0 \\ 0 & 0 \end{bmatrix} \begin{bmatrix} x_s \\ \dot{x}_s \end{bmatrix} + \begin{bmatrix} 0 & 0 \\ \sigma_r & 0 \end{bmatrix} \begin{bmatrix} f_{cs} \\ f_e^* \end{bmatrix} \quad (3.16)$$

In the four-channel bilateral teleoperation architecture, the master and slave control commands can be written as

$$f_{cm} = C_m x_m + C_1 x_s + C_2 f_e \quad (3.17)$$

$$f_{cs} = C_s x_s + C_3 x_m + C_4 f_h \quad (3.18)$$

where C_m and C_s are local master and slave controllers. C_1 , C_2 , C_3 and C_4 are position and force channel teleoperation controllers.

Under ideal conditions, the four-channel controller can provide perfect transparency by rendering the interface between the operator and environment to a rigid tool without dynamics [15].

Traditional teleoperation controllers have constant control parameters. Unfortunately, it is often difficult to find a set of parameters that performs satisfactory both in free motion and in contact with a rigid environment. While the controller's

damping must be large in rigid contact to prevent oscillatory behavior, this additional damping would create a sluggish feeling in free motion. The significant change in the environment dynamics during the transition from free motion to rigid contact and visa versa limits the achievable performance by fixed-gain controllers. The next section presents a multi-model control technique to tackle this problem.

3.3 Multiple Model State Estimation and Control for Teleoperation

Multiple model state estimation and control have been proposed for hybrid systems. Such systems involve a combination of evolving continuous states and abrupt state jumps [82,83]. The continuous states of a linear hybrid system evolve according to the following model [82]

$$x(k+1) = F[M(k)]x(k) + G[M(k)]u(k) + v[k, M(k)] \quad (3.19)$$

$$z(k) = H[M(k)]x(k) + I[M(k)]u(k) + \omega[k, M(k)] \quad (3.20)$$

where $M(k)$, the discrete state, denotes the model of system at time k . $x(k+1)$ and $x(k)$ are the systems' continuous states at times $k+1$ and k , respectively. $u(k)$ is a known input at time k and $z(k)$ is the observation vector. F , G , H and I are the state transition and observation matrices of the system which depend on the discrete state $M(k)$. v and ω are process and measurement noise vectors which can also be function of the discrete state. The mode of operation at time k is assumed

to be among finite r possible modes, i.e.

$$M(k) \in \{M_j\}_{j=1}^r \quad (3.21)$$

A full probabilistic description of the system requires knowledge about the current state, as well as all the predecessor states. For the special suboptimal case of discrete first-order and time invariant Markov chain, this probability description is truncated to just the current state [84]. It will be assumed that the mode jump process is a Markov process with known mode transition probabilities [82].

$$p_{ij} = P\{M(k) = M_j | M(k-1) = M_i\} \quad (3.22)$$

and p_{ij} is the probability of switching from mode i at time $k-1$ to mode j at time k .

Several suboptimal methods have been used in multiple model state estimation for hybrid systems. The generalized pseudo-Bayesian (GPB) approaches combine histories of models that differ in prior time steps. In particular, the first-order GPB (GPB1), which is used in this thesis, only considers the possible models in the current time step [82].

The GPB1 assumes (see Fig. 3.1) that the knowledge about the system history prior to time k is summarized in the state estimate $\hat{x}(k-1|k-1)$ and its associated covariance $P(k-1|k-1)$. The algorithm invokes a Kalman filter for each possible mode at the current time step to obtain mode-based estimates of the continuous

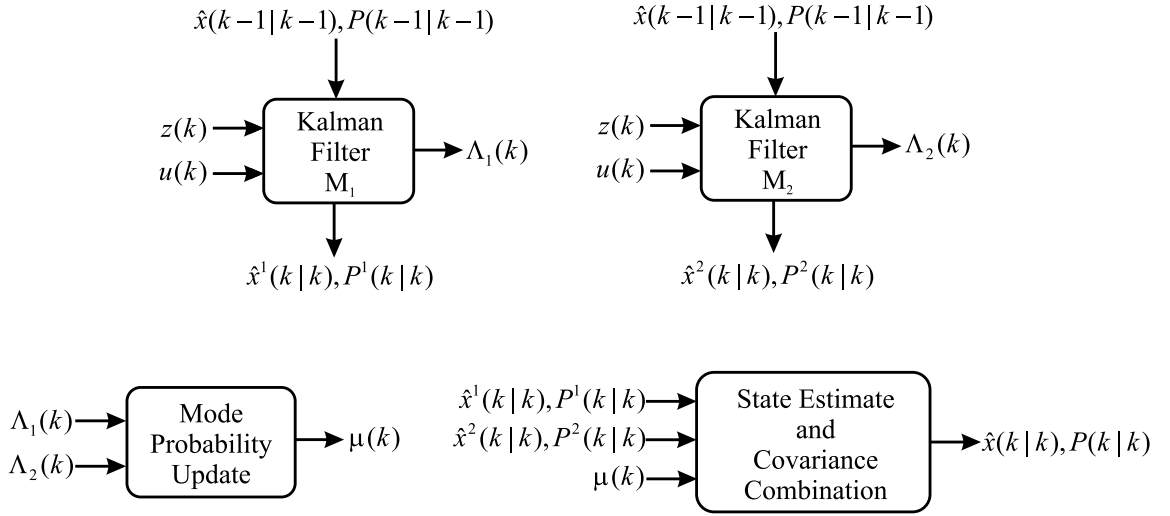


Figure 3.1: GPB1 method for two models.

states $\hat{x}^j(k|k)$ and their covariance matrix $P^j(k|k)$. It then combines the mode-based estimates using mode probabilities to estimate the continuous states, i.e.

$$\hat{x}(k|k) = \sum_{j=1}^r \mu_j(k) \hat{x}^j(k|k) \quad (3.23)$$

The definition of $\mu_j(k)$ will follow. The covariance of $\hat{x}(k|k)$ is

$$P(k|k) = \sum_{j=1}^r \mu_j(k) \{P^j(k|k) + [\hat{x}^j(k|k) - \hat{x}(k|k)][\hat{x}^j(k|k) - \hat{x}(k|k)]'\} \quad (3.24)$$

The likelihood of observation $z(k)$ given the previous estimated state $\hat{x}(k-1|k-1)$ and the current model $M_j(k)$ is

$$\Lambda_j(k) = p[z(k)|M_j(k), \hat{x}(k-1|k-1), P(k-1|k-1)] \quad (3.25)$$

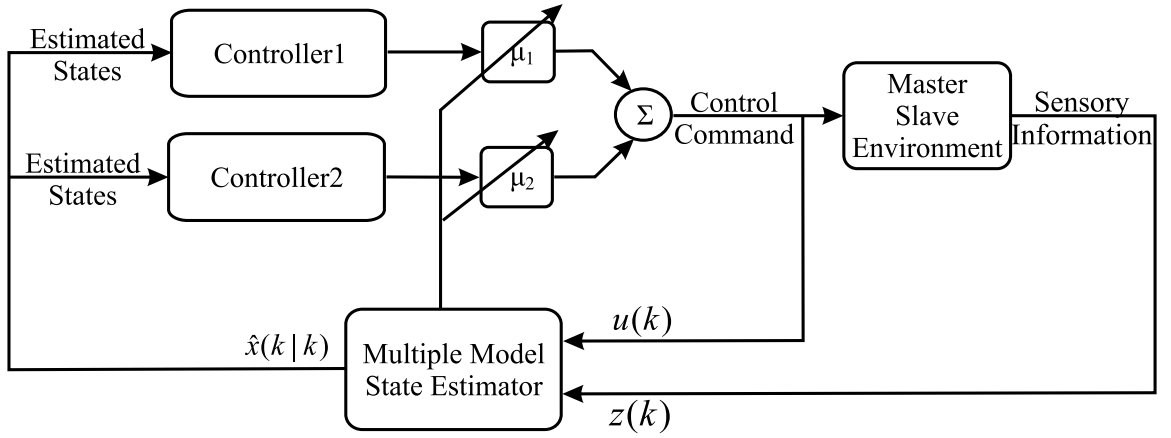


Figure 3.2: Multiple model state estimation and control for two modes.

and the probability of mode j being the actual mode at time k is

$$\mu_j(k) = \frac{1}{c} \Lambda_j(k) \sum_{i=1}^r p_{ij} \mu_i(k-1) \quad (3.26)$$

where c is a normalization factor, i.e.

$$c = \sum_{j=1}^r \Lambda_j(k) \sum_{i=1}^r p_{ij} \mu_i(k-1) \quad (3.27)$$

Mode-based controllers are designed for different modes of operation. For example in the case of teleoperation, one controller can be used when the slave is in free motion and another controller is employed for rigid contact. The overall control signal is the probability-weighted average of the mode-based control outputs as displayed in Figure 3.2 [44,85], i.e.

$$f_c = \sum_{j=1}^r \mu_j f_{cj} \quad (3.28)$$

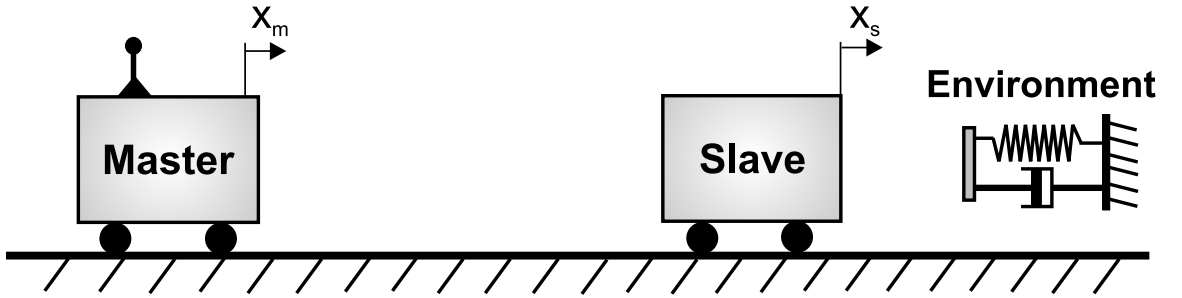


Figure 3.3: Schematic of the single-axis teleoperation system.

where f_{c_j} is the control command generated by the controller associated with the j^{th} model and μ_j is the probability of this mode being the effective mode at the present time step.

3.4 Simulation Results

The proposed multi-model teleoperation control method is applied to a single-axis four-channel bilateral teleoperation system, the schematic of which is shown in Figure 3.3. Numerical simulations are first performed to evaluate the controller and more importantly tune its parameters for the experiments. The system parameters used in the simulations are given below. The system parameters reflect those of the experimental setup. The master and slave robots are dynamically and kinematically similar.

System parameters:

$$\begin{aligned} m_m &= 3.5 & b_m &= 2.2 & k_m &= 0.1 \\ m_s &= 3.5 & b_s &= 1.6 & k_s &= 0.1 \end{aligned} \tag{3.29}$$

Simple proportional-derivative position controllers at master and slave sides

along with unity force feed-forward gains provide transparency according to [23]. The master and slave positions would track each other and the operator would interact with the environment through the tool dynamics. However, as the environment's stiffness increases the system's poles will approach the imaginary axis and the system will exhibit a highly oscillatory response. In practice, this causes the slave robot to bounce against a rigid environment. Adding damping to the master and slave during the contact phase can reduce these oscillations and stabilize the system's behavior. To be effective, this extra damping should be added not only during the contact but also in a small vicinity of the contact point. Otherwise, insufficient energy is dissipated due to the very short period of hard contact and actuator saturation. In summary, three modes of operation are identified as follows:

Mode 1: The slave robot is in free motion. The slave dynamics and the observation equation in continuous time can be written as

$$\begin{bmatrix} \dot{x}_s \\ \ddot{x}_s \\ \dot{x}_0 \end{bmatrix} = \begin{bmatrix} 0 & 1 & 0 \\ -\frac{k_s}{m_s} & -\frac{b_s}{m_s} & 0 \\ 0 & 1 & 0 \end{bmatrix} \begin{bmatrix} x_s \\ \dot{x}_s \\ x_0 \end{bmatrix} + \begin{bmatrix} 0 \\ \frac{1}{m_s} f_{cs} \\ 0 \end{bmatrix} \quad (3.30)$$

$$\begin{bmatrix} x_s \\ f_e \end{bmatrix} = \begin{bmatrix} 1 & 0 & 0 \\ 0 & 0 & 0 \end{bmatrix} \begin{bmatrix} x_s \\ \dot{x}_s \\ x_0 \end{bmatrix} \quad (3.31)$$

where x_s is the slave position. f_e and f_{cs} are the environment and slave controller forces, respectively. m_s , k_s and b_s are mass, stiffness and damping of the slave

robot. The environment rest position x_0 is considered as part of the state vector and is equal to the slave position in this mode. Environment force which is one of the measurements is zero in free motion. The continuous dynamic equations stated in (3.30) and (3.31) can be discretized using a zero-order hold approximation. After adding process and observation noise to the dynamics, a set of discrete dynamic equations similar to those in (3.19) and (3.20) are obtained.

The four-channel mode-based control laws are

$$f_{cm1} = K_{cm}(x_m - x_s) + B_{cm}(\dot{x}_m - \dot{x}_s) + f_e \quad (3.32)$$

$$f_{cs1} = K_{cs}(x_m - x_s) + B_{cs}(\dot{x}_m - \dot{x}_s) + f_h \quad (3.33)$$

where K and B are controllers' proportional and differential coefficients, respectively.

Mode 2: The slave is in contact with a rigid environment. The continuous time dynamics of slave are governed by

$$\begin{bmatrix} \dot{x}_s \\ \ddot{x}_s \\ \dot{x}_0 \end{bmatrix} = \begin{bmatrix} 0 & 1 & 0 \\ -\frac{k_s+k_e}{m_s} & -\frac{b_s+b_e}{m_s} & \frac{k_s+k_e}{m_s} \\ 0 & 0 & 0 \end{bmatrix} \begin{bmatrix} x_s \\ \dot{x}_s \\ x_0 \end{bmatrix} + \begin{bmatrix} 0 \\ \frac{1}{m_s} \\ 0 \end{bmatrix} f_{cs} \quad (3.34)$$

$$\begin{bmatrix} x_s \\ f_e \end{bmatrix} = \begin{bmatrix} 1 & 0 & 0 \\ k_e & b_e & -k_e \end{bmatrix} \begin{bmatrix} x_s \\ \dot{x}_s \\ x_0 \end{bmatrix} \quad (3.35)$$

where k_e and b_e are the stiffness and damping of the environment the slave is interacting with. Environment rest position x_0 is constant in this mode, i.e. $\dot{x}_0 = 0$. Note that the environment reaction force is given by

$$f_e = K_e(x_s - x_0) + B_e\dot{x}_s \quad (3.36)$$

The control law for this mode includes an extra local damping for master and slave:

$$f_{cm2} = K_{cm}(x_m - x_s) + B_{cm}(\dot{x}_m - \dot{x}_s) + f_e + B_{cme}\dot{x}_m \quad (3.37)$$

$$f_{cs2} = K_{cs}(x_m - x_s) + B_{cs}(\dot{x}_m - \dot{x}_s) + f_h + B_{cse}\dot{x}_s \quad (3.38)$$

where B_{cme} and B_{cse} are the local damping coefficients added to stabilize the contact behavior.

Mode 3: The slave enters this mode right after the first contact with the rigid environment and exits the mode once it is beyond Δx of the contact point. The dynamics of slave are the same as those in free motion except that the environment rest position x_0 is constant. The control law in this mode also includes the extra damping, i.e. $f_{cm3} = f_{cm2}$ and $f_{cs3} = f_{cs2}$.

Mode transition probabilities in (3.22) are chosen such that the slave can switch from Mode 1 to Mode 2 but not Mode 3. It is also possible to move back and forth between Modes 2 and 3. However, the slave can only enter Mode 1 from Mode 3 (see Figure 3.4). The overall control command for the system is calculated according to (3.28).

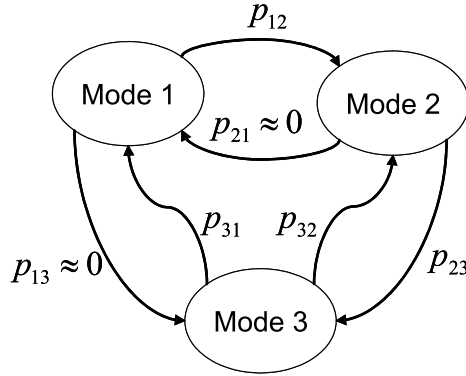


Figure 3.4: Mode transition probabilities

$$f_{cm} = \mu_1 f_{cm1} + \mu_2 f_{cm2} + \mu_3 f_{cm3} \quad (3.39)$$

$$f_{cs} = \mu_1 f_{cs1} + \mu_2 f_{cs2} + \mu_3 f_{cs3} \quad (3.40)$$

Remark: The environment rest position x_0 is unknown and is estimated using the sensory information. One may argue that the contact with rigid environment can be detected by monitoring the environment force measurement. However, this is not an effective strategy due to chattering in force during rigid contact. Furthermore, in some applications the slave may interact with soft environments as well as hard environments and the controller must differentiate between the two. The proposed approach can accommodate for such cases by incorporating models for soft contact. Although the environment stiffness k_e is used in the model, the approach was found to be robust with respect to the choice of k_e . Therefore, the exact value of the environment stiffness is not needed in the design and a typical value can be used.

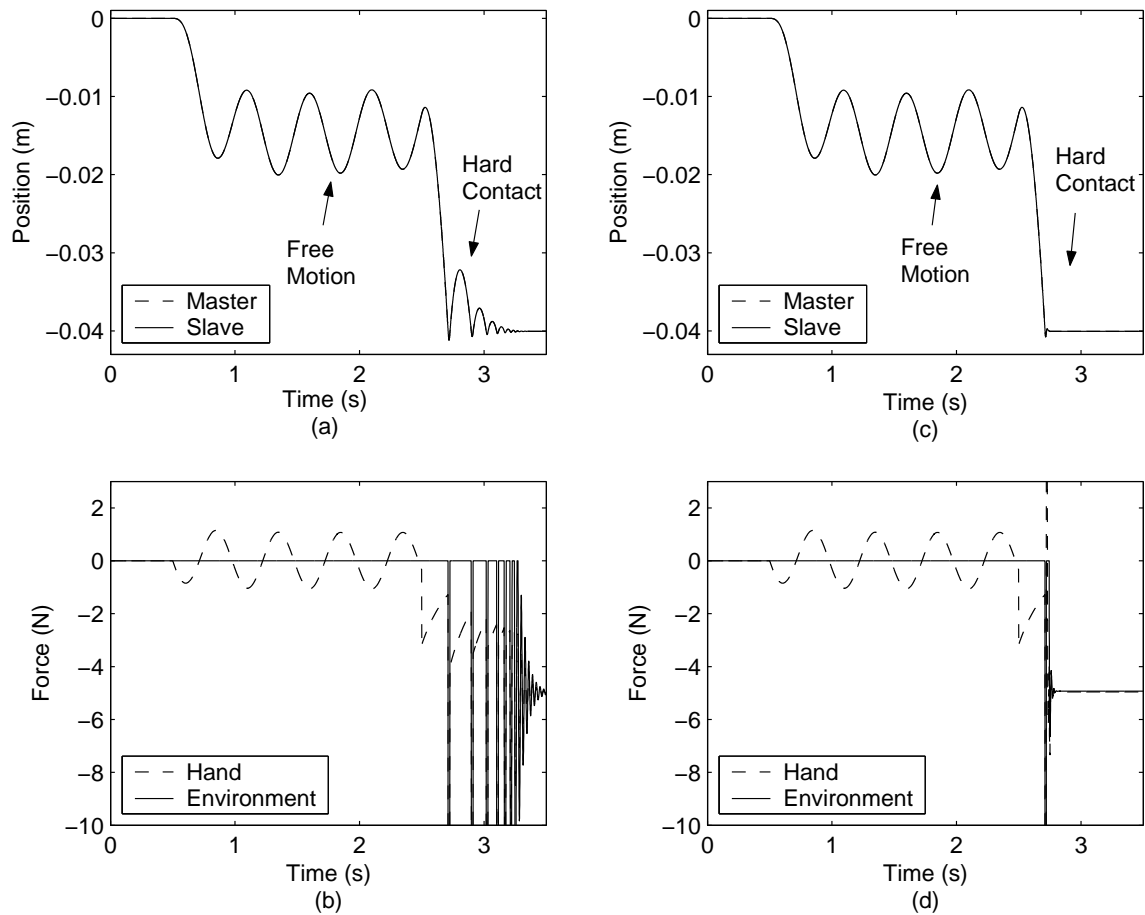


Figure 3.5: Position and force tracking in simulation: (a), (b) fixed-gain controller (c), (d) multi-model controller.

Numerical simulations were performed to evaluate the effectiveness of the multi-model teleoperation controller as compared with a fixed-gain four-channel controller. Figure 3.5(a) displays the position tracking of the fixed-gain controller where the master and slave accurately track each other in free motion. Nevertheless, the slave bounces a few times as it hits the rigid wall. In contrast, the multi-model controller performs well both in free motion and in rigid contact as demonstrated in Figures 3.5(c) and (d). The fast and effective detection of the rigid

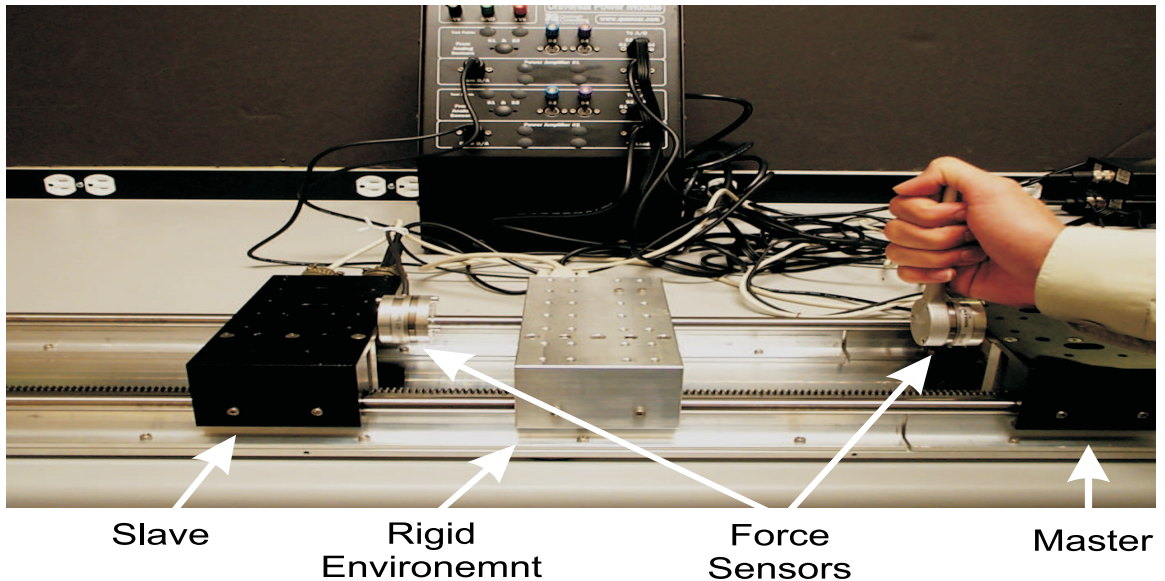


Figure 3.6: The experimental setup.

contact has resulted in a noticeable improvement in the contact behavior that can be observed in Figure 3.5(d).

3.5 Experimental Results

Figure 3.6 depicts the master-slave teleoperation experimental setup. It consists of two linear carts powered by DC motors employed as master (right) and slave (left). The middle cart is clamped to the track and is used as a rigid wall. Angular movement of the motor shafts are transformed to linear movement using a rack and pinion structure. The motors are equipped with optical encoders that produce 4096 pulses per revolution. This yields a linear position measurement resolution of 9.74×10^{-6} m. Master and slave carts are equipped with *ATI* force sensors to measure the operator and environment forces. The control system runs on a PC platform using *VxWorks* real-time operating system at 2048 Hz. The control code

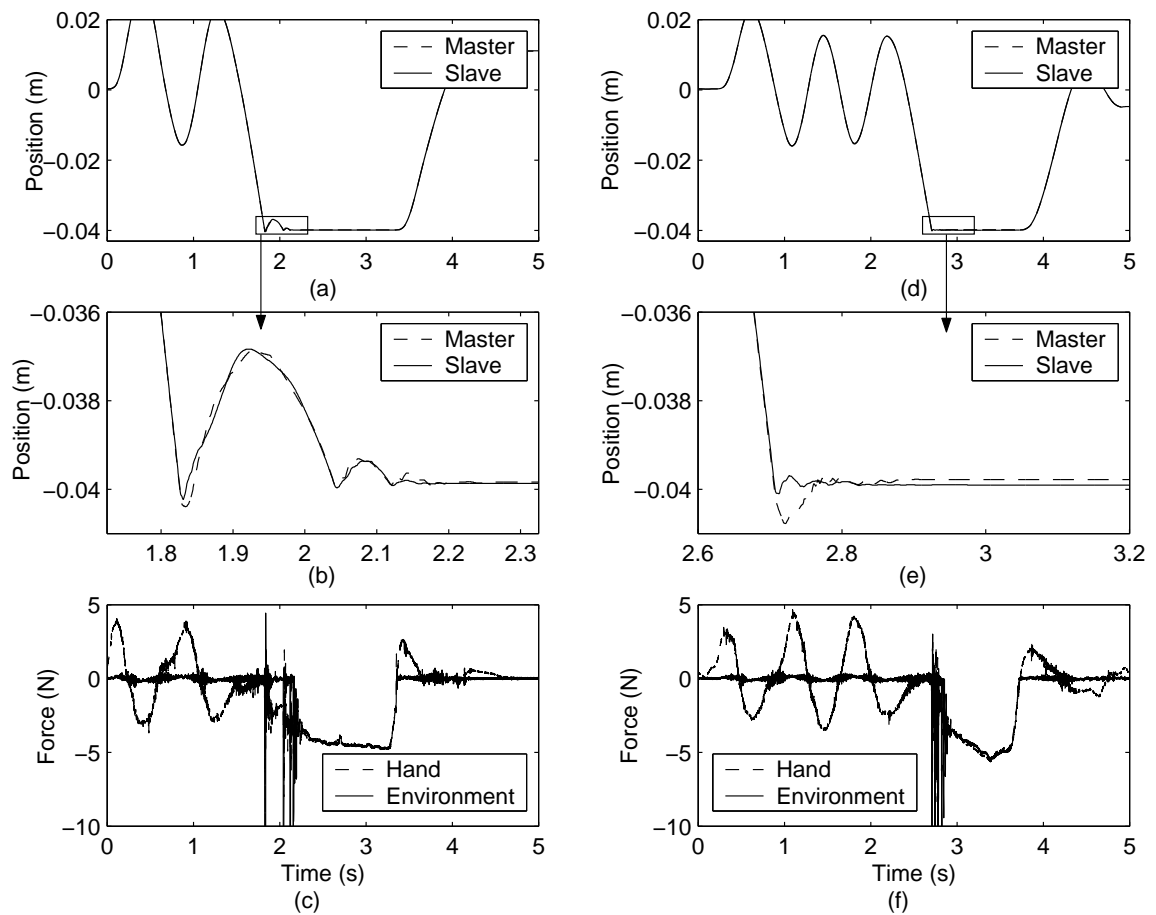


Figure 3.7: Position and force tracking in experiment: (a),(b),(c) fixed-gain controller (d),(e),(f) adaptive multi-model controller.

is implemented by *Matlab Real-time Workshop* toolbox.

Experiments were conducted using the simulation scenario and parameters. Figures 3.7(a) and 3.7(d) illustrate that both fixed-gain and adaptive controller perform well in free motion. However, the adaptive controller clearly outperforms the fixed-gain controller in rigid contact by reducing the slave bounces against the wall. This is evident by comparing Figures 3.7(b) and (e) that zoom in the hard contact period.

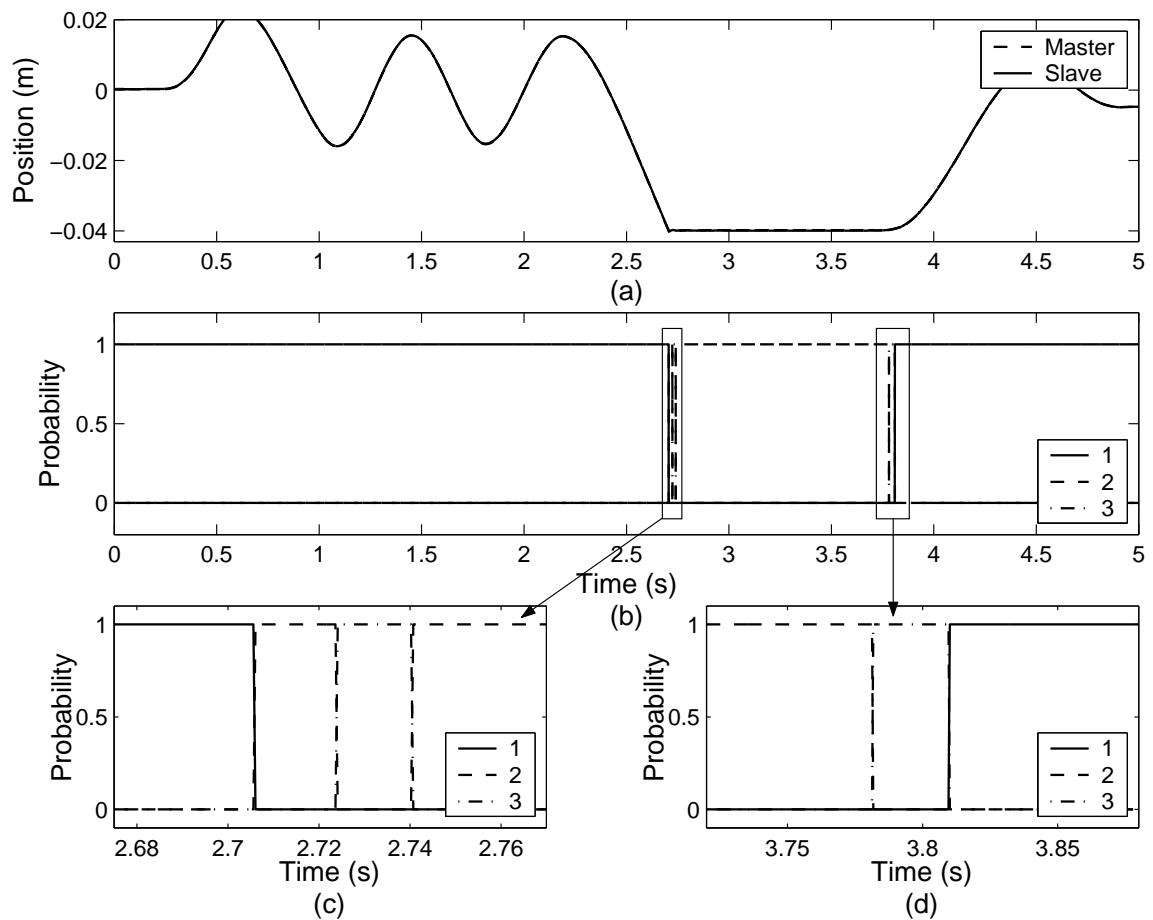


Figure 3.8: Mode probability transitions in experiment.

Figure 3.8 shows the mode probabilities during the experiment with the multi-model controller. Mode 1 probability is close to one when the slave is in free motion before and after contact. While the slave is in contact, Mode 2 is dominant and its probability is almost 1. Two transitions occur in the probabilities first when the slave hits the wall and next when it leaves the wall. The mode probabilities during these transitions are plotted in Figures 3.8(c) and (d). In the first transition, the slave hits the wall (transition from Mode 1 to Mode 2) and bounces back (Mode 2 to Mode 2) and again hits the wall (Mode 3 to Mode 2) (see Figure 3.8(c)). Since

the bounce is less than Δx , the slave does not enter the free motion mode. In the second transition when slave leaves the contact, first the system's mode alters from 2 to 3. After the slave leaves the Δx zone, the system enters the free motion mode (Mode 1) (see Figure 3.8(d)).

Chapter 4

Discrete-Time LQG Teleoperation Controller

4.1 Introduction

This chapter deals with the delay problem in teleoperation. To this end a bilateral teleoperation controller based on the Linear Quadratic Gaussian control is proposed. The main contributions of this method are: (i) the explicit incorporation of the communication time delay into the system model and control synthesis; (ii) the formulation of the teleoperation control as an LQG optimal control design. The performance indices used include non-delayed position tracking, force tracking, and virtual tool impedance shaping. The proposed approach allows for the systematic optimization of the transparency measures while maintaining stability. Linearized dynamics of master and slave are the same as those derived in the previous chapter. The LQG control problem is stated in Section 4.2. A single-axis teleoperation design example along with numerical simulations are presented in

Section 4.3. In Section 4.4, a robust stability analysis of the proposed controller is performed. Experimental results are given in Section 4.5.

4.2 LQG Teleoperation Control

The performance of conventional single-master/single-slave telerobotic systems is measured by their transparency. In an ideally transparent telerobotic system, the operator should feel that he/she is directly interacting with the environment. This notion of transparency, also denoted as ideal kinesthetic coupling [23], can be described in terms of position and force tracking between the master and slave robots [14,23]:

$$f_h = \alpha_f f_e \quad (4.1)$$

$$x_m = \alpha_p x_s \quad (4.2)$$

where α_f and α_p scale the force and position tracking between the master and slave. Acceleration measurement or equivalently force measurement, and the exact knowledge of the master and slave dynamics are required for achieving the ideal transparency. Unfortunately in a perfectly transparent system, modelling errors can cause instability because of the complete cancellation of the master and slave dynamics (e.g. a negative mass can be produced) [23]. A modified version of transparency defines a virtual intervening tool between the operator and the

environment [14,23], i.e.

$$f_h = m_t \ddot{x}_m + b_t \dot{x}_m + k_t x_m + \alpha_f f_e \quad (4.3)$$

$$x_m = \alpha_p x_s \quad (4.4)$$

where m_t , b_t , and k_t are mass, damping, and stiffness of the virtual tool. While in a transparent system according to (4.1)-(4.2) the operator interacts with the task environment through a rigid tool without dynamics, the modified transparency measures introduce an intervening virtual tool with desired mass-spring-damper dynamics. The tool parameters should be selected such that sufficient stability margins are gained without compromising the operator's perception of the environment through a dominant tool dynamics. It should be noted that in rigid contact, the modified transparency requirements in (4.1)-(4.2) reduce to original force and position tracking measures in (4.1)-(4.2), if $k_t = 0$.

The system dynamics in (3.3), (3.8), (3.12) and the performance indices in (4.1)-(4.4) are all expressed in the continuous-time domain. In practice, the system outputs are sampled and the control actions are applied at a fixed rate. The control signal is constant between the sampling instants. The transformation of the dynamics and the performance measures into the discrete-time domain allows for direct discrete control synthesis. The application of a zero-order-hold continuous to discrete transformation [16] results in the following dynamics for the operator/master subsystem:

$$X_m[n+1] = A_m X_m[n] + B_m f_{cm}[n] + G_m w_m[n] \quad (4.5)$$

where $X_m[n] = \begin{bmatrix} x_m[n] & v_m[n] \end{bmatrix}^T$ is the state vector. The control signal $f_{cm}[n]$ has been introduced in (3.1) and the disturbance signal is $w_m[n] = \begin{bmatrix} f_h^*[n] & \tilde{f}_{cm}[n] \end{bmatrix}^T$ where $\tilde{f}_{cm}[n]$ is the disturbance in the control signal $f_{cm}[n]$.

Similarly, the slave/environment dynamics can be written as

$$X_s^i[n+1] = A_s^i X_s^i[n] + B_s^i f_{cs}[n] + G_s^i w_s[n] \quad i = 1, 2, 3 \quad (4.6)$$

where indices 1, 2, 3 correspond to free motion, contact with a flexible environment, and contact with a rigid environment, respectively; $X_s^{1,2}[n] = \begin{bmatrix} x_s[n] & v_s[n] \end{bmatrix}^T$ while $X_s^3[n] = f_e[n]$. The control signal is $f_{cs}[n]$ and the disturbance vector is $w_s[k] = \begin{bmatrix} f_e^*[n] & \tilde{f}_{cm}[n] \end{bmatrix}^T$. The state transition matrices are a function of the contact state i . Note that in rigid contact the slave robot's state is the environment force $f_e[n]$. In practice, the controller implementation introduces one sample delay and hence $f_e[n] = f_{cs}[n-1]$. The desired tool dynamics in (4.3) can also be converted to the discrete-time domain

$$X_t[n+1] = A_t X_t[n] + B_t u_t[n] \quad (4.7)$$

where $X_t[n] = \begin{bmatrix} x_t[n] & v_t[n] \end{bmatrix}^T$ and $u_t[n] = \begin{bmatrix} f_h[n] & f_e[n] \end{bmatrix}^T$.

Teleoperation controllers are often distributed between the master and slave sites due to the distribution of system dynamics. In such an architecture, the master controller receives non-delayed position/force information from the master and delayed position/force information from the slave. On the other hand, the slave controller uses non-delayed data from the slave and delayed information

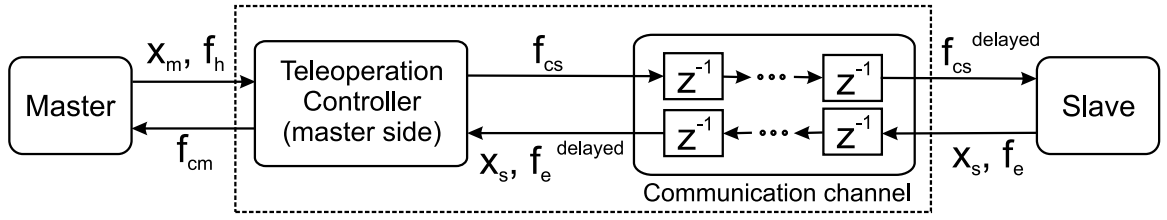


Figure 4.1: Teleoperation controller resides at the master side.

from the master. Nevertheless, the LQG control is a centralized design approach which utilizes all measurements in generating the control signals. Therefore, controller must be placed either at the master end or at the slave end. Throughout this thesis it is assumed that the controller resides at the operator end (see Figure 4.1).

The structural change in the slave/environment dynamics due to rigid contact and parameter variations due to flexible contact can be handled with a multi-model control approach [43,86]. Mode-based controllers are designed for different phases of the operation. Switching between these controllers occurs according to the estimated contact state. In this strategy, a controller is designed for free motion; another controller handles flexible contacts while a third controller is employed for interacting with rigid environments. Alternatively, it is possible to design a single controller that can function for both free motion and flexible contact, although such an approach would be more conservative.

4.2.1 Free motion/soft contact

The states of the system for the cases of free motion/soft contact are defined as follows

$$X[n] = \begin{bmatrix} \alpha_p X_s[n] - X_m[n] & X_m[n] - X_t[n] & X_t[n] \end{bmatrix}^T \quad (4.8)$$

where $X_m[n]$, $X_s[n]$, and $X_t[n]$ have been introduced in (4.5), (4.6) and (4.7); α_f and α_p have been defined in (4.3) and (4.4). The above choice of states facilitates the application of the LQG method by explicitly including the tracking errors of interest into the state vector. The states evolution is governed by

$$X[n + 1] = AX[n] + Bu[n] + Gw[n] \quad (4.9)$$

and

$$u[n] = \begin{bmatrix} f_{cm}[n] & f_{cs}[n] \end{bmatrix}^T \quad (4.10)$$

$$w[n] = \begin{bmatrix} f_h^*[n] & f_e^*[n] & \tilde{f}_{cm}[n] & \tilde{f}_{cs}[n] \end{bmatrix}^T \quad (4.11)$$

It is straightforward to obtain the system matrices, A , B , G from A_m , B_m , C_m , D_m , G_m , H_m , A_s , B_s , C_s , D_s , G_s , H_s , A_t , and B_t . The measurement vector is

$$y[n] = \begin{bmatrix} y^1[n] & y^2[n - d] \end{bmatrix}^T \quad (4.12)$$

$$y^1[n] = \begin{bmatrix} x_m[n] & f_h[n] \end{bmatrix}^T \quad (4.13)$$

$$y^2[n - d] = [\alpha_p x_s[n - d] - x_m[n - d], f_e[n - d], \\ x_m[n - d] - x_t[n - d], v_t[n - d]]^T \quad (4.14)$$

where d is the communication latency in number of sample times. These observations are generated based on the actual sensors' readings $x_m[n]$, $f_h[n]$, $x_s[n]$, and $f_e[n]$ as well as the intervening tool model in (4.7) (see Figure 4.2). The measurement vector in (4.12) is particularly suited for the LQG design as it contains the

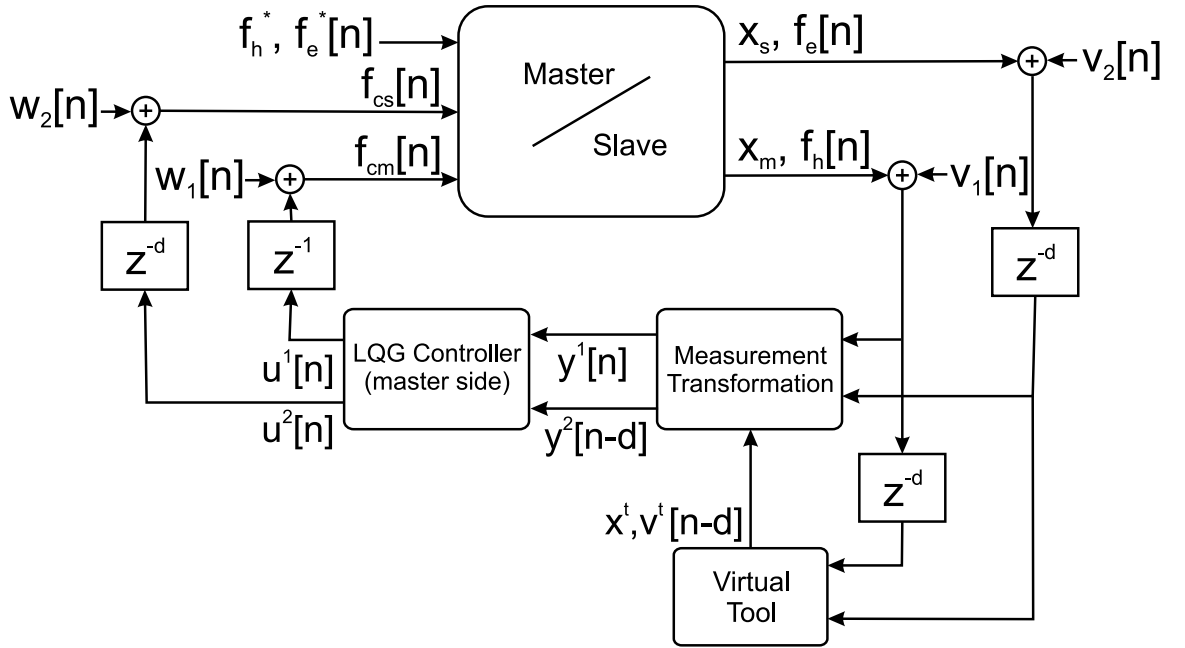


Figure 4.2: The LQG teleoperation control system.

delayed tracking errors. The delayed measurements will eventually be incorporated into the system states as will be seen shortly. Note that the slave and tool measurements are delayed by d samples. The rationale is obvious in the case of the slave measurements as the controller is implemented at the master side and it would take d samples before that the slave information arrive at the master end. The virtual tool observations $x_t[n - d]$, and $v_t[n - d]$ which are produced by the control algorithm are also delayed since they depend on the environment force $f_e[n - d]$.

Part of the observation vector in (4.12), i.e. $y^2[n - d]$ can not be directly written in terms of the system's states and inputs in (4.8) and (4.9) due to the existence of the delay. Nonetheless, the treatment of the problem in the discrete-time domain allows for the incorporation of time delay via a finite number of states into

the system's model. The delayed measurement vector is produced by passing the original non-delayed signals through d unit delay blocks. The outputs of the unit delay blocks are added to the system's states. The non-delayed observation vectors $y^1[n]$ and $y^2[n]$ can be written in terms of the states and the control actions in (4.8)-(4.9),

$$y^1[n] = C^1 X[n] + D^1 u[n] + H^1 w[n] + v^1[n] \quad (4.15)$$

$$y^2[n] = C^2 X[n] + D^2 u[n] + H^2 w[n] + v^2[n] \quad (4.16)$$

where $v^1[n]$ and $v^2[n]$ are measurement noise; $X[n]$, $u[n]$, and $w[n]$ have been introduced before. The new augmented state vector is given by

$$X_n[n] = \left[X[n] \quad y^2[n-1] \quad y^2[n-2] \quad \cdots \quad y^2[n-d] \right]^T \quad (4.17)$$

and the corresponding system matrices are

$$A_n = \begin{bmatrix} A & 0 & 0 & \cdots & 0 \\ C^2 & 0 & 0 & \cdots & 0 \\ 0 & I & 0 & \cdots & 0 \\ \vdots & & & & \vdots \\ 0 & \cdots & \cdots & I & 0 \end{bmatrix}, B_n = \begin{bmatrix} B \\ D^2 \\ 0 \\ \vdots \\ 0 \end{bmatrix} \quad (4.18)$$

$$C_n = \begin{bmatrix} C^1 & 0 & \cdots & 0 \\ 0 & \cdots & 0 & I \end{bmatrix}, D_n = \begin{bmatrix} D^1 \\ 0 \end{bmatrix} \quad (4.19)$$

$$G_n = \begin{bmatrix} G & 0 \\ H^2 & I \\ 0 & 0 \\ \vdots & \vdots \\ 0 & 0 \end{bmatrix}, H_n = \begin{bmatrix} H^1 & 0 \\ 0 & 0 \end{bmatrix} \quad (4.20)$$

Also, the new process and measurement noise vectors are

$$w_n[n] = \begin{bmatrix} w[n] & v^2[n] \end{bmatrix}^T \quad (4.21)$$

$$v_n[n] = \begin{bmatrix} v^1[n] & 0 \end{bmatrix}^T \quad (4.22)$$

The input and output remain unchanged, i.e. $u[n]$, and $y[n]$. The master and slave control actions are subject to time delay as well. The delays for the master and slave control signals are one and d samples, respectively.

$$u[n] = \begin{bmatrix} f_{cm}[n] & f_{cs}[n] \end{bmatrix}^T = \begin{bmatrix} u^1[n-1] & u^2[n-d] \end{bmatrix}^T \quad (4.23)$$

The delay in control signals can be included in the model by augmenting the states as follows

$$\bar{X}[n] = \left[X_n[n] \quad u^1[n-1] \quad u^2[n-d] \quad u^2[n-d+1] \quad \cdots \quad u^2[n-1] \right]^T \quad (4.24)$$

The new system matrices are

$$\bar{A} = \begin{bmatrix} A_n & B_n^1 & B_n^2 & 0 & 0 & \cdots & 0 \\ 0 & 0 & 0 & 0 & 0 & \cdots & 0 \\ 0 & 0 & 0 & 1 & 0 & \cdots & 0 \\ 0 & 0 & 0 & 0 & 1 & \cdots & 0 \\ \vdots & & & & & & \vdots \\ 0 & \cdots & & & & & 0 \end{bmatrix}, \quad \bar{B} = \begin{bmatrix} 0 & 0 \\ 1 & 0 \\ 0 & 0 \\ 0 & 0 \\ \vdots & \vdots \\ 0 & 1 \end{bmatrix} \quad (4.25)$$

$$\bar{C} = \left[C_n \quad D_n^1 \quad D_n^2 \quad 0 \quad \cdots \quad 0 \right], \quad \bar{D} = 0 \quad (4.26)$$

$$\bar{G} = \begin{bmatrix} G_n \\ 0 \\ \vdots \\ 0 \end{bmatrix}, \quad \bar{H} = H_n \quad (4.27)$$

and the new input vector is

$$\bar{u}[n] = \left[u^1[n] \quad u^2[n] \right]^T \quad (4.28)$$

The output, process noise, and measurement noise are not changed.

The operator's exogenous force $f_h^*[n]$ is part of the disturbance vector $w_n[n]$.

This signal can be modelled by a stochastic process and added to the system's states. This approach would enable the real-time estimation of the force based on the sensory observations. A first-order model is used, i.e.

$$f_h^*[n+1] + \alpha_{fh}f_h^*[n] = n_f[n] \quad (4.29)$$

where α_{fh} is a constant and $n_f[n]$ is a white Gaussian sequence. The final discrete-time state-space representation of the system after the augmentation of f_h^* into the state vector is given by

$$X_f[n+1] = A_fX_f[n] + B_fu_f[n] + G_fw_f[n] \quad (4.30)$$

$$y_f[n] = C_fX_f[n] + H_fw_f[n] + v_f[n] \quad (4.31)$$

and

$$X_f[n] = \begin{bmatrix} \bar{X}[n] & f_h^*[n] \end{bmatrix}^T \quad (4.32)$$

$$y_f[n] = y_n[n] = \begin{bmatrix} y^1[n] & y^2[n-d] \end{bmatrix}^T \quad (4.33)$$

$$u_f[n] = \bar{u}[n] = \begin{bmatrix} u^1[n] & u^2[n] \end{bmatrix} \quad (4.34)$$

$$w_f[n] = \begin{bmatrix} n_f[n] & f_e^*[n] & \tilde{f}_{cm}[n] & \tilde{f}_{cs}[n] & v^2[n] \end{bmatrix}^T \quad (4.35)$$

$$v_f[n] = v_n[n] = \begin{bmatrix} v^1[n] & 0 \end{bmatrix}^T \quad (4.36)$$

The system matrices are

$$A_f = \begin{bmatrix} \bar{A} & \bar{G}(:, 1) \\ 0 & -\alpha_{fh} \end{bmatrix}, B_f = \begin{bmatrix} \bar{B} \\ 0 \end{bmatrix} \quad (4.37)$$

$$C_f = \begin{bmatrix} \bar{C} & \bar{H}(:, 1) \end{bmatrix}, D_f = \bar{D} \quad (4.38)$$

$$G_f = \begin{bmatrix} 0 & \bar{G}_{12} & \cdots & \bar{G}_{18} \\ \vdots & \cdots & \vdots & \\ 0 & \bar{G}_{5d+7 \ 1} & \cdots & \bar{G}_{5d+7 \ 8} \\ 1 & 0 & \cdots & 0 \end{bmatrix} \quad (4.39)$$

$$H_f = \begin{bmatrix} 0 & \bar{H}_{12} & \cdots & \bar{H}_{18} \\ \vdots & \vdots & & \\ 0 & \bar{H}_{62} & \cdots & \bar{H}_{68} \end{bmatrix} \quad (4.40)$$

where $\bar{G}(:, 1)$ and $\bar{H}(:, 1)$ denote the first columns of \bar{G} and \bar{H} matrices, respectively.

4.2.2 Rigid contact

When the slave is in rigid contact, its continuous-time dynamics are governed by (3.12)-(3.14) with their discrete-time equivalent given in (4.6). In this case, the vector of discrete states including the master and slave subsystems is chosen as

$$X[n] = \begin{bmatrix} x_m[n] - \alpha_p x_s[n] & v_m[n] & x_s[n] & f_e[n] \end{bmatrix}^T \quad (4.41)$$

and the measurement vector is

$$y[n] = \begin{bmatrix} y^1[n] & y^2[n-d] \end{bmatrix}^T \quad (4.42)$$

$$y^1[n] = \begin{bmatrix} x_m[n] & f_h[n] \end{bmatrix} \quad (4.43)$$

$$y^2[n-d] = \begin{bmatrix} x_m[n-d] - \alpha_p x_s[n-d] & f_h[n-d] - \alpha_f f_e[n-d] \end{bmatrix}^T \quad (4.44)$$

This leads to a discrete-time difference equation similar to the one in (4.9) with the following transition matrices

$$A = \begin{bmatrix} A_m & \alpha_p(A_m^{11} - 1) & 0 \\ & \alpha_p A_m^{21} & \\ 0 & \beta & 0 \\ 0 & 0 & 0 \end{bmatrix}, \quad B = \begin{bmatrix} B_m & 0 \\ 0 & 0 \\ 0 & 1 \end{bmatrix} \quad (4.45)$$

and

$$u[n] = \begin{bmatrix} f_{cm}[n] & f_{cs}[n] \end{bmatrix}^T \quad (4.46)$$

$$w[n] = \begin{bmatrix} f_h^*[n] & \tilde{f}_{cm}[n] & \tilde{f}_{cs}[n] & w_{xs}[n] \end{bmatrix}^T \quad (4.47)$$

Note that the slave position in rigid contact $x_s[n]$ is modelled by

$$x_s[n+1] = \beta x_s[n] + w_{xs}[n] \quad (4.48)$$

with $\beta \rightarrow 1^-$ and $w_{xs}[n]$ is a white Gaussian sequence. The steps to incorporate the delay in the measurements and the control signals as well as the operator's exogenous force $f_h^*[n]$ into the system's states are similar to those in the previous case and will not be repeated here. The dynamics of the augmented system in the discrete-time domain can be expressed by the following difference equations

$$X_r[n+1] = A_r X_r[n] + B_r u_r[n] + G_r w_r[n] \quad (4.49)$$

$$y_r[n] = C_r X_r[n] + D_r u_r[n] + H_r w_r[n] + v_r[n] \quad (4.50)$$

with

$$X_r[n] = \left[X[n] \quad y^2[n-1] \quad \cdots \quad y^2[n-d] \quad u^2[n-d] \quad \cdots \quad u^2[n-1] \quad f_h^*[n] \right]^T \quad (4.51)$$

$$y_r[n] = y[n] \quad (4.52)$$

$$w_r[n] = \begin{bmatrix} n_f[n] & \tilde{f}_{cm}[n] & \tilde{f}_{cs}[n] & w_{xs}[n] & v^2[n] \end{bmatrix} \quad (4.53)$$

$$v_r[n] = \begin{bmatrix} v^1[n] & 0 \end{bmatrix} \quad (4.54)$$

It should be noted that the one sample delay in the master control action has already been added to $X[n]$ in (4.41).

4.2.3 LQG control design

The system dynamics and measurement equations in (4.30)-(4.31) for free motion/soft contact and in (4.49)-(4.50) for rigid contact are in the standard form for

the application of the LQG control synthesis. The deterministic inputs to the system are the master and slave control signals $u_f[n]$, $u_r[n]$. The system is also perturbed by the stochastic inputs $w_f[n]$, $w_r[n]$ which are assumed zero mean white Gaussian sequences. The measurement noise vectors $v_f[n]$, $v_r[n]$ are also zero mean white Gaussian signals. The LQG controller attempts to minimize the effect of the stochastic disturbance inputs on the states through minimizing the following loss function for $N \rightarrow \infty$ [16]

$$J(u) = \frac{1}{N} E \left\{ \sum_{n=1}^N X[n]^T Q X[n] + u[n]^T R u[n] + 2X^T[n] \Gamma u[n] \right\} \quad (4.55)$$

where $E\{\cdot\}$ denotes the expected value, and $Q \geq 0$, $R > 0$. The optimal controller is a combination of a constant state feedback gain obtained from solving the corresponding deterministic optimal Linear Quadratic (LQ) control and an optimal *Kalman* filter state estimator, i.e.

$$u[n] = -K \hat{X}[n|n-1] \quad (4.56)$$

where the feedback gain K is given by

$$K = (B^T S B + R)^{-1} (B^T S A + \Gamma^T) \quad (4.57)$$

and S is the solution to the following Discrete-time Algebraic *Riccati* Equation (DARE)

$$A^T S A - S - (A^T S B + \Gamma)(B^T S B + R)^{-1}(B^T S A + \Gamma^T) + Q = 0 \quad (4.58)$$

The state estimate $\hat{X}[n|n-1]$ is the output of a *Kalman* filter with the following dynamics

$$\hat{X}[n+1|n] = A\hat{X}[n|n-1] + Bu[n] + L(y[n] - C\hat{X}[n|n-1] - Du[n]) \quad (4.59)$$

The *Kalman* filter gain L is computed as follows

$$L = APC^T (\Pi + CPC^T)^{-1} \quad (4.60)$$

where P is the solution to the following DARE

$$APA^T - P - APC^T (\Pi + CPC^T)^{-1} CPA^T + W = 0 \quad (4.61)$$

where $W = E \{Gw[n]w[n]^T G^T\}$ and $\Pi = E \{v[n]v[n]^T\}$ are the covariances of the process and measurement noise, respectively. Certain conditions must be satisfied for the existence of a solution to the LQG problem. These include the stabilizability of pair (A, B) and detectability of pair (C, A) among others. It can be shown that the teleoperation system satisfies all necessary requirements.

The special form of the system states for free motion/soft contact and the rigid contact facilitates the LQG design for achieving the teleoperation performance objectives. For free motion/soft contact one may write:

$$X_f[n]^T Q_f X_f[n] = \sum_{k=0}^d q_{1k} (\alpha_p x_s[n-k] - x_m[n-k])^2 + q_{2k} (x_m[n-k] - x_t[n-k])^2 \quad (4.62)$$

with $q_{1k} > 0$ and $q_{2k} > 0$. Similarly for rigid contact,

$$X_r[n]^T Q_r X_r[n] = \sum_{k=0}^d q_{1k} (x_m[n-k] - \alpha_p x_s[n-k])^2 + \sum_{k=1}^d q_{2k} (f_h[n-k] - \alpha_f f_e[n-k])^2 \quad (4.63)$$

We assume $\Gamma = 0$ in (4.55). The schematic of the proposed LQG teleoperation control system is displayed in Figure 4.2. The sensor measurements are the master and slave positions as well as the hand and environment forces. Delayed hand and environment force signals are used to generate delayed virtual tool position and velocity. These synthesized observations along with the actual transformed/delayed observations enter the LQG controller block at the master site which in turn produces the master and slave control signals using the algorithm described above. The control signals are then transmitted to the master and slave actuators.

Remark 4.1: The quadratic terms in (4.62) and (4.63) involve position and force tracking errors at concurrent sample times. Therefore, despite the presence of $2d$ samples round trip delay, the controller attempts to produce non-delayed position and force tracking. Intuitively, this is achieved through the prediction of master and slave motions by model-based *Kalman* filters. Also, the matrices Q_f and Q_r are positive semi-definite as opposed to positive definite. This is critical for the design of the teleoperation controller since the system must be allowed to move freely. Therefore, only the tracking errors are penalized in (4.55) and the gains corresponding to the rest of the states in Q 's are set to zero.

Remark 4.2: The disturbance terms in the model, in particular $f_h^*[n]$ and $f_e^*[n]$, can

introduce tracking errors and hence degrade the performance. The effect of these disturbances can be attenuated by tightening the feedback loops through increasing Q and/or decreasing R in (4.55). However, large feedback gains can amplify the noise and reduce the system's stability margins. The inclusion of $f_h^*[n]$, and similarly $f_e^*[n]$ if needed, in the state vector through the first-order model (4.29) can further attenuate the tracking errors as it allows for the real-time estimation of $f_h^*[n]$. Nevertheless, such model may not accurately predict the operator's exogenous force for a long prediction horizon. More complex force generation models can be employed to further increase the prediction horizon of the controller.

Remark 4.3: Models of operator, master robot, slave robot, and environment dynamics are used by the controller. While the master and slave parameters are often known and constant, the operator and environment dynamics are usually unknown and time-varying. The controllers are designed based on the nominal values of the operator and environment parameters. Variation in these parameters can degrade the performance and may even cause instability. Nevertheless, the results of simulations, analysis and experiments presented later, demonstrate that a careful selection of the LQG design parameters can render the system sufficiently robust w.r.t. operator and environment parameter changes.

Remark 4.4: Controllers are designed for different phases of the operation, e.g. free motion, contact with flexible environments, and contact with rigid environments. Multi-model estimation techniques [43, 86, 87] can be employed to identify the mode of operation and to apply the corresponding controller.

Remark 4.5: The order of controller is equal to the system's order, i.e. $5d + 8$ for

free motion/flexible contact and $3d + 6$ for rigid contact. The number of sample delays d depends on the control frequency and the communication latency. The order of controller can become large in some applications. However, it turns out that the controller possesses a sparse structure that can be exploited for its efficient implementation, if needed. It is also possible to adopt a multi-rate control strategy where the teleoperation controller runs at a slower rate than that of the local feedback linearizing controllers. A reduced-order version of the controller is introduced in chapter 5.

Remark 4.6: The proposed control approach can be employed in case of time-varying delay by introducing buffers that store measurement and control signals at the master and slave ends. The time-delay is rendered constant by adding artificial delay to these signals if and when necessary.

4.3 Simulation Results

The proposed LQG control scheme is applied to the single-axis bilateral teleoperation system introduced in chapter 3 (see figure 3.3). The controller is implemented at the master side. The operator manipulates the slave robot in free motion and in contact with a rigid environment. Two different controllers are designed. The first controller is intended for free motion operation and the second controller handles rigid contact. Multiple-model controller, introduced in chapter 3 of this thesis, is used to handle the changes in environment, i.e. employing the correct controller for each mode of operation.

The system parameters are the same as those used in chapter 3 (see (3.29)).

Additional system parameters, such as tool parameters and control parameters are given below. Typical values for the arm's mass, damping, and stiffness are employed in the controller design.

Additional system parameters:

$$\begin{aligned}
 m_t &= 3 & b_t &= 6 & k_t &= 0.01 \\
 m_h &= 0.35 & b_h &= 0.1 & k_h &= 0.02 \\
 m_e &= 0.04 & b_e &= 1 & k_e &= 0.1 \\
 \alpha_f &= 1 & \alpha_p &= 1 & \alpha_{fh} &= 0.999
 \end{aligned} \tag{4.64}$$

LQG parameters for free motion controller:

$$\begin{aligned}
 q_{1i} &= \begin{cases} 10^6 & i = d \\ 0 & \text{otherwise} \end{cases} \\
 q_{2i} &= \begin{cases} 5 \times 10^5 & i = d \\ 0 & \text{otherwise} \end{cases} \\
 R &= \text{diag}(0.1, 0.1) \\
 E\{w_f w_f^T\} &= \text{diag}(0.1, 4, 0.1, 0.1, 10^{-8}, 10^{-4}, 10^{-8}, 10^{-6}) \\
 E\{v_f v_f^T\} &= \text{diag}(10^{-8}, 10^{-4}, 0, 0, 0, 0)
 \end{aligned}$$

LQG parameters for rigid contact:

$$q_{1i} = \begin{cases} 5 \times 10^6 & i = d \\ 0 & \text{otherwise} \end{cases}$$

$$q_{2i} = \begin{cases} 1 & i = d \\ 0 & \text{otherwise} \end{cases}$$

$$R = \text{diag}(0.1, 0.1)$$

$$\beta = 0.999$$

$$E\{w_r w_r^T\} = \text{diag}(1, 0.01, 0.01, 10^{-9}, 10^{-8}, 10^{-4})$$

$$E\{v_r v_r^T\} = \text{diag}(10^{-8}, 10^{-4}, 0, 0)$$

All values are expressed in the metric units. The controller performance and its robustness w.r.t. parameter variations are examined through various simulation scenarios. These include teleoperation under different communication delays with matched and mismatched parameters. Delay is introduced in the slave position and force information as well as the slave control signal since the controller is implemented at the master end.

(i) Simulations with matched parameters:

In this case, the system parameters used in the LQG design are the same as those employed to simulate master, slave, and environment dynamics. Three different levels of round trip time delay are examined, i.e. 125ms, 250ms, and 500ms. Figure 4.3 shows the position and force tracking results. Note that the second figure in each of the columns is an enlarged version of the rigid-contact transient

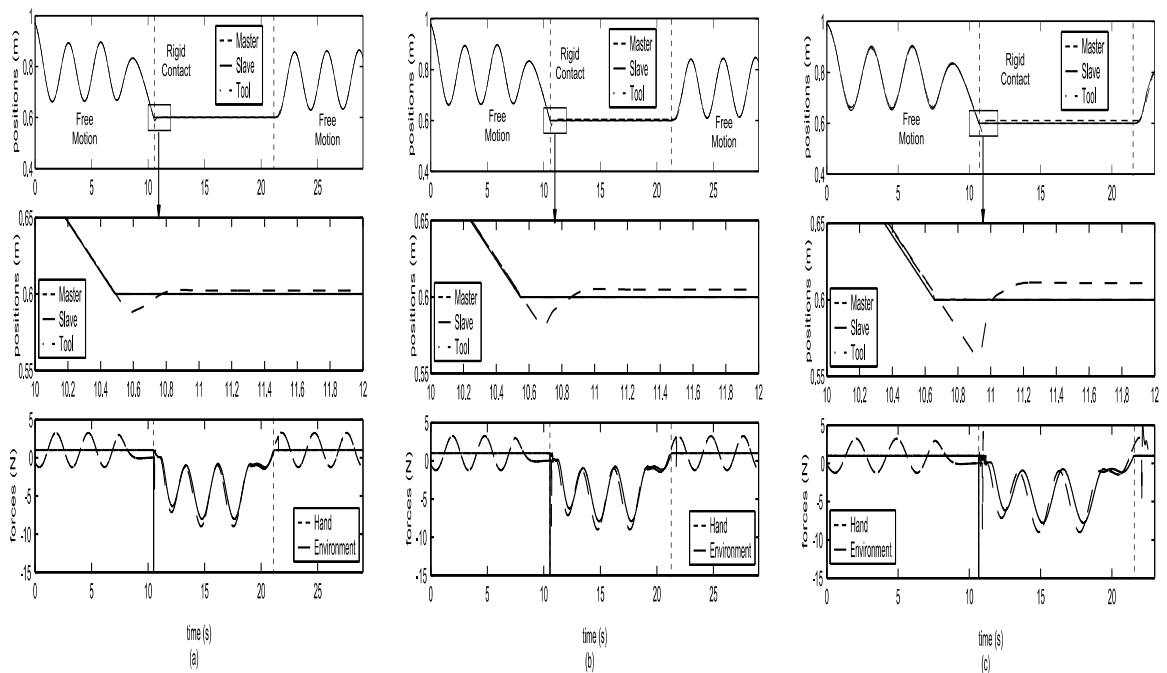


Figure 4.3: Position and force tracking in simulation for matched parameters: (a) 125ms delay (b) 250ms delay (c) 500ms delay.

designated by a rectangle in the first figure in the column. The rigid mode signal indicates when the rigid (one) or free motion (zero) mode controller is being used. The LQG controller demonstrates excellent position tracking and impedance shaping in free motion. Note that the positions of master and slave closely follow that of the virtual tool without delay. The controller uses the model information to compensate for the delay through prediction. The tracking error slightly increases as latency becomes larger. This demonstrates the effect of uncertainties such as the operator's exogenous force and measurement noise, included in the simulations, on the system's performance.

The controller exhibits stable contact transition from free motion to rigid contact and vice versa. There is a delay in force tracking during the rigid contact. This

is due to the fact that first-order model for operator's exogenous force f_h^* in (4.29) can not accurately predict its behavior. The operator perceives a rigid contact despite a small discrepancy between master and slave positions. This is evident from the master position plot which shows a constant master position despite the variations in the applied hand force. The force oscillation in the rigid contact is due to the operator's intentional hand force and is meant to display the force tracking capability of the controller.

(ii) Simulations with mismatched parameters:

The simulations were repeated, this time with mismatched parameters. The master and slave parameters can be estimated with high accuracy. The design example requires no environment parameter as it considers free motion and rigid contact. However, the arm parameters are unknown and can vary from one operator to another. It was discovered through simulation and experimentation that the system is most sensitive to the operator's arm mass. Figure 4.4 displays the results for the case in which there is a 600% error in the mass, i.e. $m_h(\text{real})= 0.05\text{kg}$ and $m_h(\text{model})= 0.35\text{kg}$. The LQG controller still demonstrates accurate force and position tracking with stable contact behavior for all three levels of time delay despite the large parameter mismatch as is evident in this figure. Simulations were also conducted for the case in which $m_h(\text{real})= 1\text{kg}$ and $m_h(\text{model})= 0.35\text{kg}$. The system became unstable for 500ms round-trip delay while the responses were quite satisfactory for delays of 125 and 250ms.

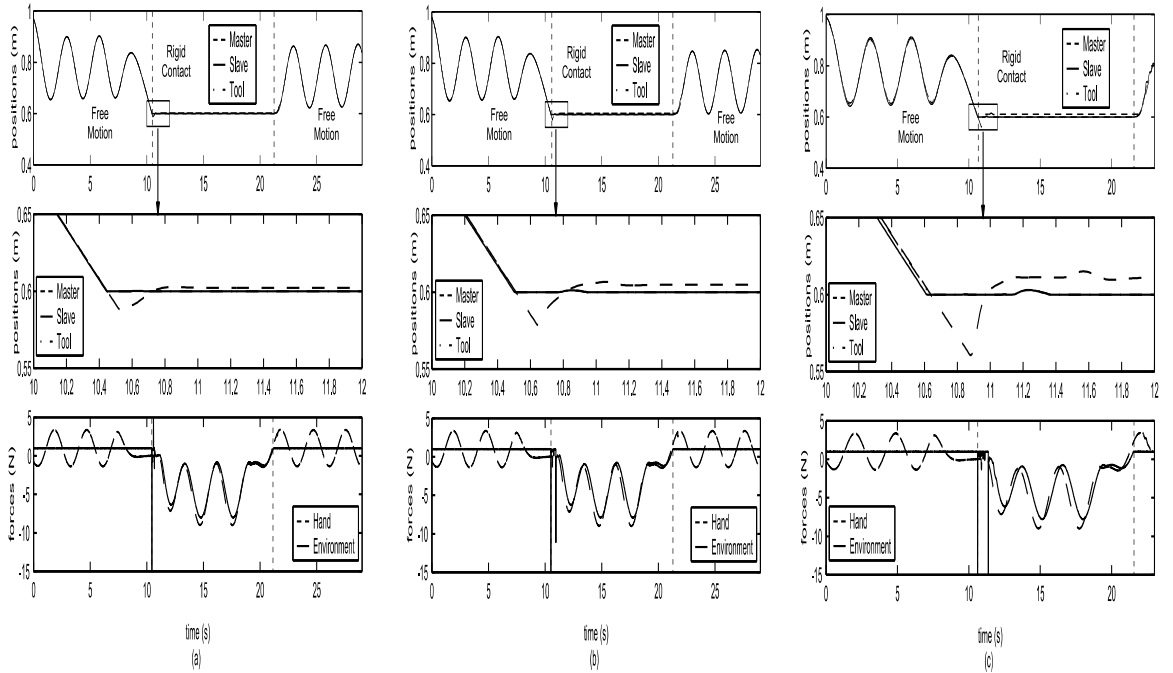


Figure 4.4: Position and force tracking in simulation for mismatched model parameters: (a) 125ms delay (b) 250ms delay (c) 500ms delay.

4.4 Robust Stability Analysis

The proposed multiple-model LQG controller is a model-based approach that requires the parameters of master, slave, operator, and the environment (in soft contact). The robustness of the controller was demonstrated through a few numerical simulation scenarios in the previous section. It is also possible to investigate this robustness via classical linear analysis tools such as the *Nyquist* theorem. To avoid complications of a multi-variable analysis, we study the robustness with respect to changes in individual parameters separately. In each case, the controller/observer and all system parameters are fixed except one parameter of interest. The *Nyquist* analysis is then employed to obtain the value of parameter for which the system becomes marginally stable.

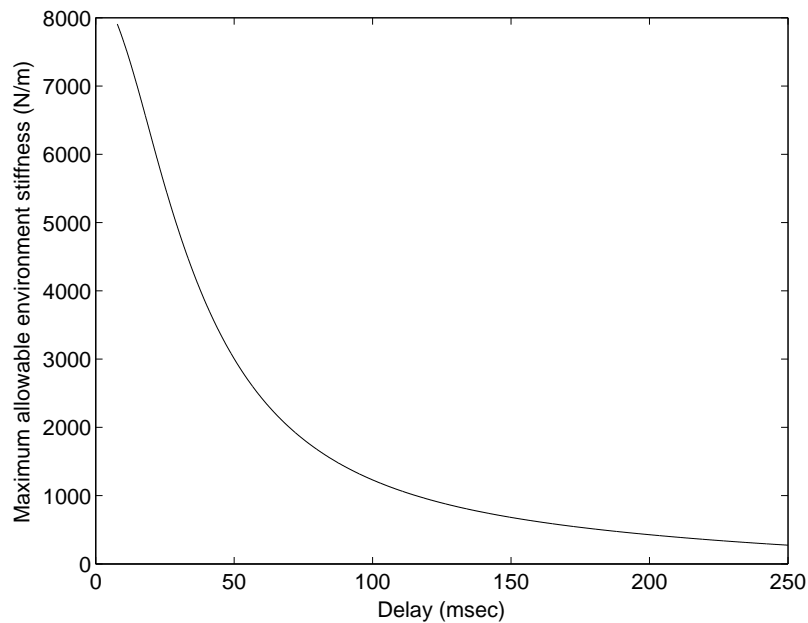


Figure 4.5: Robustness of free motion controller w.r.t. mismatch in environment stiffness ($k_e = 0.1$ in design).

4.4.1 Robustness against mismatch in environment stiffness

The environment stiffness in the design of the free motion controller was assumed 0.1N/m . The free motion controller could also be used to interact with soft environments. Obviously, this will introduce uncertainty in the form of environment stiffness in the system's dynamics. In Figure 4.5, the maximum allowable environment stiffness for the controller with the parameters given in previous section, is plotted as a function of the time delay. As it may have been expected, the maximum stiffness decreases by the amount of time delay from over 8000N/m for delays less than 10ms to about 300N/m for a delay of 250ms . It should be noted that the same controller has been used to produce the results for different delays. The controller parameters can always be adjusted to balance the performance and robust stability based on the value of the delay and the application requirements.

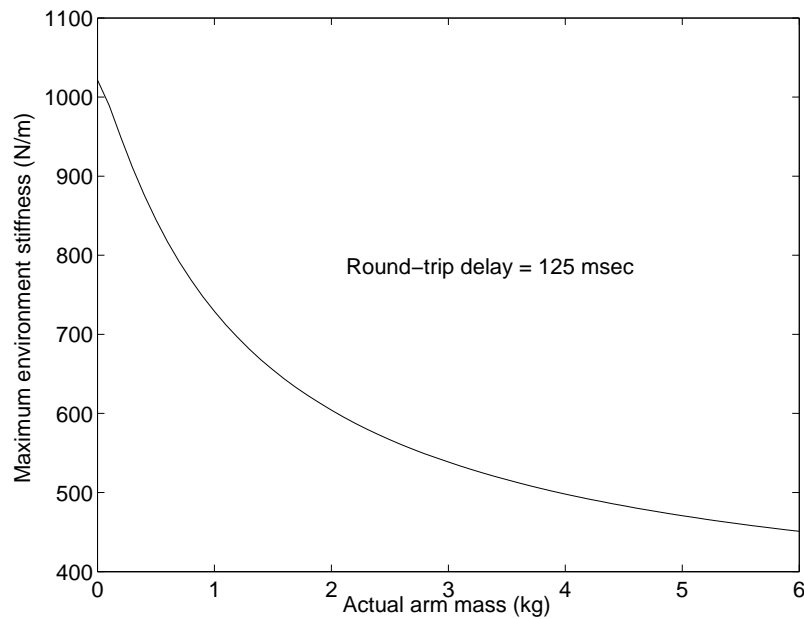


Figure 4.6: Robustness of free motion controller w.r.t. mismatch in arm mass and environment stiffness ($m_h = 0.35$ and $k_e = 0.1$ in design).

Alternatively by designing separate controllers for free motion and soft contact, system's performance and stability can be both enhanced in the expense of having a more complex controller.

4.4.2 Robustness against mismatch in arm mass and environment stiffness

The sensitivity of the free motion controller with respect to simultaneous variations in the operator's arm mass and the environment stiffness was also analyzed for a time delay of 125 ms. The results are given in Figure 4.6 where the maximum allowable environment stiffness is plotted for different values of actual arm mass. According to this figure, the maximum stiffness for the free motion controller decreases as the actual arm mass increases from more than 1000N/m for small masses

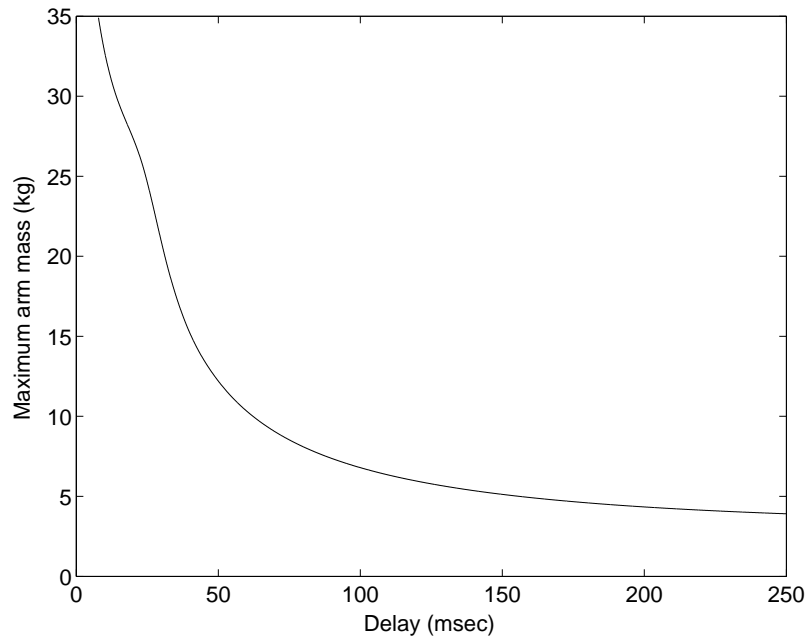


Figure 4.7: Robustness of rigid contact controller w.r.t. mismatch in arm mass ($m_h = 0.35$ in design).

to about 450N/m for $m_h = 6.0\text{kg}$. The arm mass used in the controller design is $m_h = 0.35\text{kg}$.

4.4.3 Robustness against mismatch in arm mass for rigid contact controller

The arm mass is the critical parameter in the design of the rigid contact controller. The robust stability of the controller w.r.t. variations in this parameter is demonstrated in Figure 4.7 where that maximum allowable arm mass is plotted as a function of communication delay. Again, the arm mass value used in the design is $m_h = 0.35$ kg.

In summary, it can be concluded the designed controller is fairly robust with

respect to the uncertainties considered in the analysis. Obviously, it is difficult to specify objective targets for the controller robustness margins. The designer should set the performance and robustness goals based on the application requirements and then tune the controller design parameters to achieve those objectives, if possible.

4.5 Experimental Results

Experiments are done on the same single-axis experimental setup used in chapter 3 (see figure 3.6). However, the sampling frequency here was 256 Hz.

The experiments were conducted using the simulation parameters and for three different round-trip time delays, i.e. 63ms, 125ms, and 250ms. The communication latency was emulated by adding memory buffers of appropriate size that can store and delay the slave sensory observation and control action signals. To enable comparison between the proposed controller and a standard teleoperation method, the results of experiments with a two-channel position-position controller are also reported.

4.5.1 LQG controller with 63ms delay

In Figure 4.8, the responses of the proposed controller under 63ms of communication delay are plotted. The system is initially at rest until roughly $t = 1.4\text{sec}$ when the operator begins moving the master/slave units in free motion. In this phase of operation, the operator should only feel the rendered dynamics of the virtual tool. The non-zero hand force observed in the free motion portions of Figure 4.8 is due

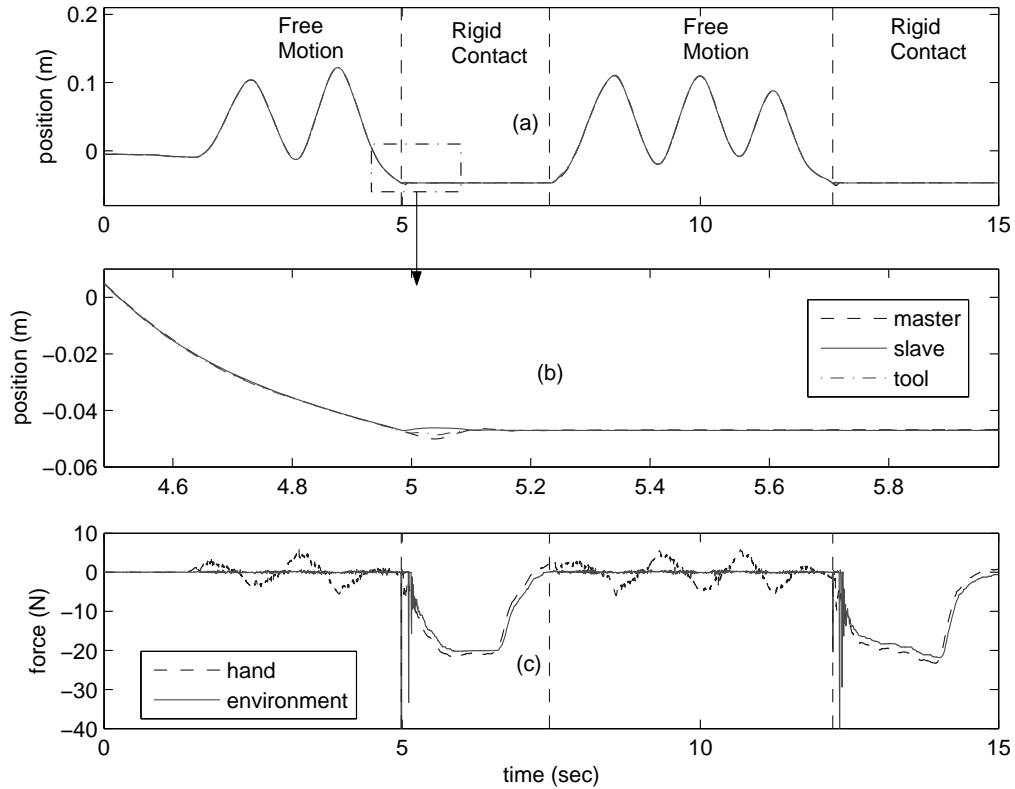


Figure 4.8: LQG controller with 63ms delay in experiment: (a) position tracking for master/slave/virtual tool; (b) contact transition (c) force tracking.

to these dynamics. The positions of master, slave, and virtual tool closely follow each other in free motion which confirms that the performance objectives in (4.3) and (4.4) are both achieved with very high precision.

At $t \simeq 5.0$ sec, the slave makes an initial contact with the rigid wall. This causes the controller to switch to the rigid mode after approximately 32ms, the time that is required for the environment force measurement to arrive at controller in the master side. There is about 0.2sec transition period before the contact becomes

stable during which two bounces occur against the wall. The switching logic enforces the rigid-mode controller during this time. At the operator's end and upon the initial contact, there is a small position tracking error which may increase by the amount of time delay and the master speed at the time of initial contact. This can be explained by the inability of the controller to predict an abrupt change in the environment characteristic from free motion to rigid contact. Nevertheless, the error is quickly eliminated by the controller. The resulting transient response was found acceptable by the operator in this case as well as the two other following cases with longer delays.

During the course of the first rigid contact from time 5.0-7.5 sec, the environment and hand forces as well as the master and slave positions closely track each other as can be seen in Figure 4.8. The contact is stable and is perceived rigid by the operator as is evident by the constant master position despite the changes in the hand force. At $t \simeq 7.5$ sec, the operator withdraws the master and consequently the master/slave system returns to free motion following a smooth transition. Finally, a second rigid contact occurs at $t \simeq 12.2$ sec.

4.5.2 LQG controller with 125ms delay

Figure 4.9 illustrates that responses of the controller for a round-trip delay of 125ms. As in the previous case, the experiment starts with the master/slave at rest, followed by a free motion operation and subsequent rigid contact and free motion phases. The transitions from free motion to rigid contact and vice versa are stable. Three bounces happen during the free-to-contact transition period which is about

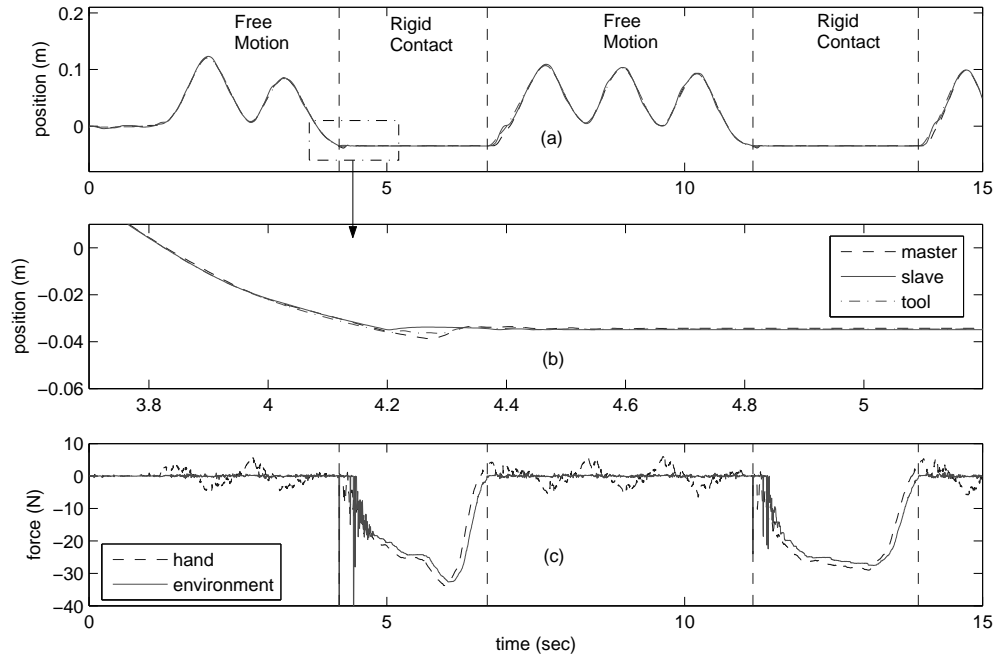


Figure 4.9: LQG controller with 125ms delay in experiment: (a) position tracking for master/slave/virtual tool; (b) contact transition (c) force tracking.

0.25 sec, slightly longer than that of the prior case. The position tracking and virtual tool rendering in free motion as well as position and force tracking in rigid contact are quite satisfactory.

4.5.3 LQG controller with 250ms delay

In Figure 4.10, the results of an experiment with the proposed teleoperation controller under 250 ms of communication latency are presented. Once again, the

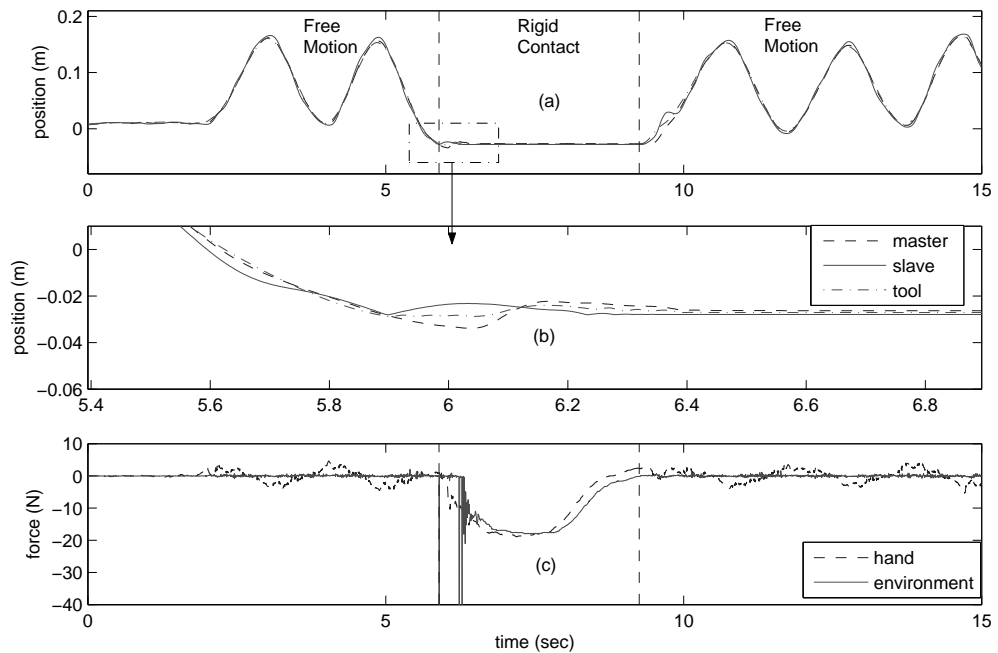


Figure 4.10: LQG controller with 250ms delay in experiment: (a) position tracking for master/slave/virtual tool; (b) contact transition (c) force tracking.

mode transitions are stable with three bounces against the wall, although the free-to-rigid transient time has increased to 0.35s in this case. The initial position tracking error during transition from free motion to rigid contact has also slightly increased. A small transient in master/slave position tracking during the rigid-to-free transition is observed which is quickly corrected by the controller. Despite slight degradation in the performance of the free motion tracking, the results are still quite satisfactory.

4.5.4 Two-channel controller with 250ms delay

A two-channel position-position [19] teleoperation controller was also implemented on our experimental setup. It is well-known that such controllers have generally larger stability margins and can tolerate longer communication delays compared with other standard techniques such as the four-channel controller [15]. The controller position and velocity error gains were manually tuned to achieve a balance between stability and performance. In this procedure, the gains were increased until an oscillatory response was observed and then slightly reduced to regain the stability. Beside the stability constraint, the operator's perceived impedance is also a limiting factor in the selection of the controller gains. Increasing the damping term could improve stability but at the same time it can render the system highly sluggish and therefore, interfere with the operator's perception of the environment.

The position and force tracking responses of the two-channel controller are displayed in Figures 4.11(a) and 4.11(b). A large position tracking error is observed both in free motion and rigid contact. The errors are specially noticeable when compared with those of the LQG controller with a similar delay in Figure 4.10. The rigid contact is perceived soft by the operator as it may have been expected from a two-channel architecture. In addition to its large tracking errors, the two-channel teleoperation controller demonstrates a sluggish response in the presence of time delay. This can be observed by comparing the level of the operator's hand forces and the amount of master/slave displacements in free motion in Figures 4.10 and 4.11. The difference is more evident in Figure 4.11(c) where the positions of the master and slave are compared with that of the desired virtual tool in the LQG

design. The difference in the responses indicates a significant departure from the desired interface impedance in free motion.

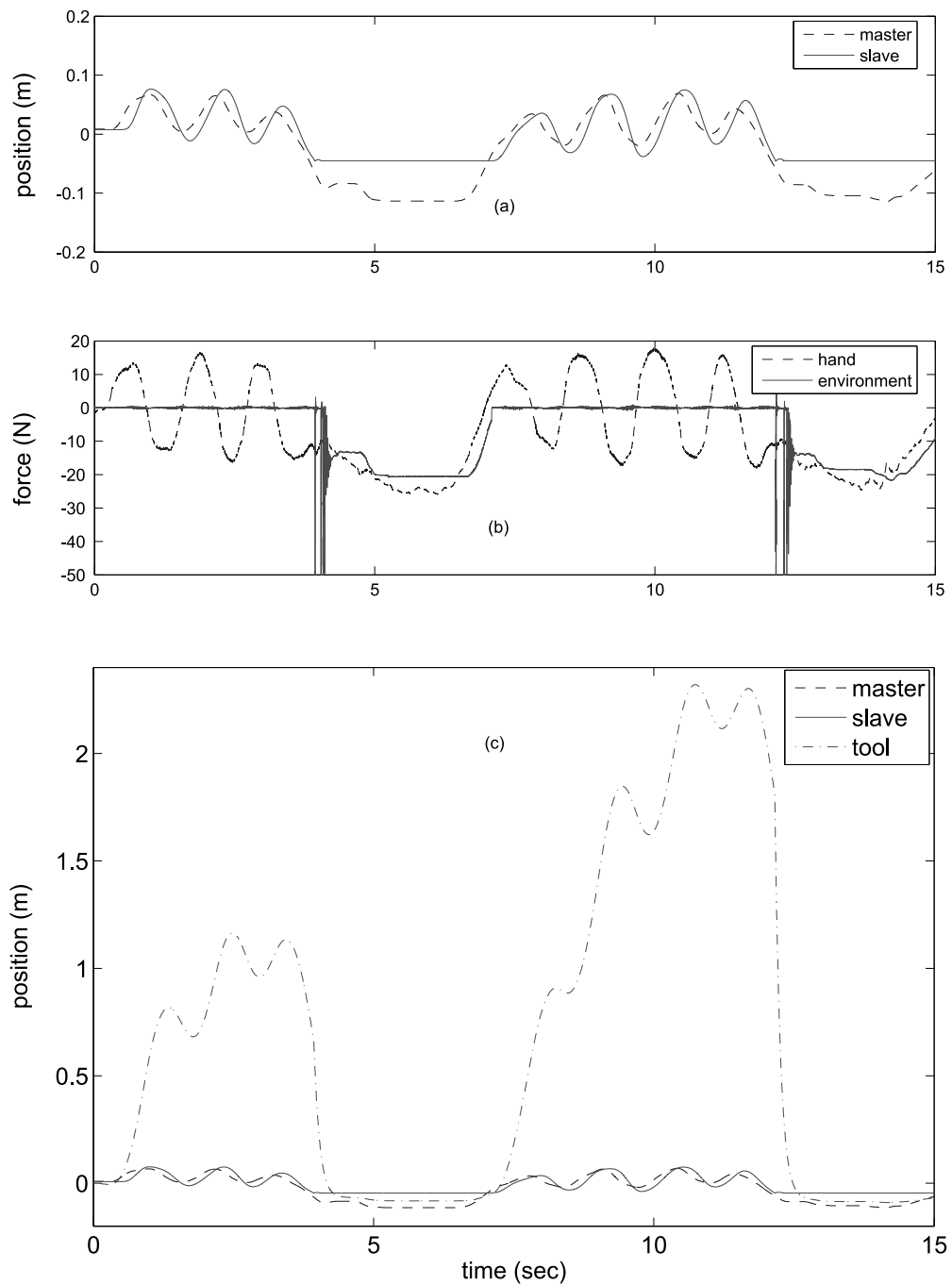


Figure 4.11: Two-channel position-position controller with 250ms delay in experiment: (a) position tracking; (b) force tracking (c) compared with desired response obtained from virtual tool.

Chapter 5

Continuous-Time LQG Teleoperation Controller

5.1 Introduction

This chapter follows on from the last chapter in which a discrete-time LQG controller for teleoperation under communication time delay was proposed. In that method, the time delay was incorporated into a finite dimension state space model of the system in the discrete time. A drawback of this method is that the number of states can grow largely as the amount of delay and control rate increase. This can limit the sampling rate for higher delays which can adversely affect the controller's performance.

Artstein [79] introduced a reduction method to change a continuous-time linear control system with delayed control actions to a control system without delay. In this manuscript, this method has been revised such that it can be applied to systems with different delays in various control and measurement channels.

This modified reduction method is then used to produce a delay-free variation of the teleoperation system dynamics. An LQG observer/controller is synthesized to achieve transparency objectives using position and force measurements at the master and slave sides. In summary, the main contributions of this method are as follows. (i) The teleoperation under time delay is formulated as a multi-model continuous-time LQG control synthesis. The performance indices used include non-delayed position tracking, force tracking and virtual tool impedance shaping. Transparency objectives are achieved by using an LQG observer/controller for the reduced system. (ii) A modified state-space reduction method for multi-input/multi-output (MIMO) control systems with dissimilar delays in measurement and control signals is proposed. It is proven that the reduced system inherits the detectability and stabilizability properties of the original system. Also, it is shown that the closed-loop stability of the reduced system guarantees the stability of the original system. The reduction transformation and predictive control for the reduced system are proposed in section 5.2. The LQG teleoperation control synthesis is discussed in section 5.3. Simulation and experimental results for various scenarios are given sections 5.4 and 5.5.

5.2 Delayed System Reduction and Control

In [79], Artstein defines a transformation to reduce an infinite dimensional system with delayed control actions to a delay-free system. Consider the multi-input/multi-output (MIMO) linear system with non-identical delays in the control signals shown

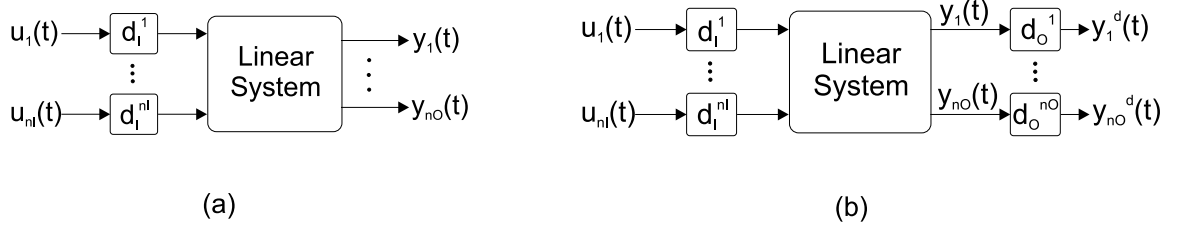


Figure 5.1: Linear system with (a) delayed control actions and (b) delayed control actions and delayed measurements

in Figure 5.1(a) with the following state space representation

$$\dot{X}(t) = AX(t) + \sum_{j=1}^{n_I} B_j u_j(t - d_I^j) + Gw(t) \quad (5.1)$$

$$y_k(t) = C_k X(t) + \sum_{j=1}^{n_I} D_{kj} u_j(t - d_I^j) + H_k w(t) + v_k(t) \quad k = 1, \dots, n_O \quad (5.2)$$

where $X(t)$ is the vector of states, $y_k(t)$ is the k 'th output vector, and $u_j(t)$ is the j th input vector; n_I and n_O are the numbers of inputs and outputs, respectively; d_I^j is the delay in the j th input channel; $w(t)$ and $v_k(t)$ are process and measurement noise, respectively. Consider the following state transformation

$$Z(t) = X(t) + \sum_{j=1}^{n_I} \int_{t-d_I^j}^t e^{A(t-s-d_I^j)} B_j u_j(s) ds \quad (5.3)$$

By taking the time derivative of (5.3) and substituting $\dot{X}(t)$ from (5.1), one may write

$$\dot{Z}(t) = AZ(t) + \sum_{j=1}^{n_I} e^{-Ad_I^j} B_j u_j(t) + Gw(t) \quad (5.4)$$

Clearly, the new system in (5.4) has no delay in control signals and therefore, standard control methods such as the state feedback control can be implemented for its stabilization. The transformation in (5.3) is only applicable to systems with delayed control signals. However in a centralized teleoperation control scheme, the controller resides at either the master or slave side, and therefore, receives non-delayed position/force information from its corresponding side and delayed position/force information from the other side. There will also be some delay in either master or slave control signal depending the location of the controller. A modified transformation is proposed here that can handle systems with different delays in their input/output channels as shown in Figure 5.1(b). Due to the presence of delay in the output channels, (5.2) is rewritten as

$$y_k^d(t) = y_k(t - d_O^k) = C_k X(t - d_O^k) + \sum_{j=1}^{n_I} D_{kj} u_j(t - h_j^k) + H_k w(t - d_O^k) + v_k(t - d_O^k) \quad (5.5)$$

where $w(t)$ and $v_k(t)$ are defined in (5.2), d_O^k is the delay in k' th output channel and h_j^k is the total delay between j' th input and k' th output, i.e.

$$h_j^k \triangleq d_I^j + d_O^k \quad (5.6)$$

The new state transformation is defined as

$$Z(t) = X(t - d_O^m) + W_m(t) \quad (5.7)$$

where $d_O^m = \max d_O^i$, $i = 1, \dots, n_O$ is the maximum latency in measurement channels and

$$W_k(t) = \sum_{j=1}^{n_I} \int_{t-h_j^k}^t e^{A(t-s-h_j^k)} B_j u_j(s) ds \quad (5.8)$$

Taking the time derivative of (5.7) and replacing $\dot{X}(t - d_O^k)$ from (5.1) yield

$$\dot{Z}(t) = A_z Z(t) + B_z u(t) + G w(t - d_O^m) \quad (5.9)$$

with

$$A_z = A \quad (5.10)$$

$$B_z = [e^{-Ah_1^m} B_1 \dots e^{-Ah_{n_I}^m} B_{n_I}] \quad (5.11)$$

For the system described in (5.1), $X(t - d_O^m)$ can be written in terms of $X(t - d_O^k)$ using standard results from the linear systems theory as follows [88]

$$X(t - d_O^m) = e^{-Ad_O^{mk}} X(t - d_O^k) - \sum_{j=1}^{n_I} \int_{t-h_j^m}^{t-h_j^k} e^{A(t-s-h_j^m)} B_j u_j(s) ds \quad (5.12)$$

where

$$d_O^{mk} = d_O^m - d_O^k \quad (5.13)$$

Replacing $X(t - d_O^m)$ in (5.7) from (5.12) results in

$$Z(t) = e^{-Ad_O^{mk}} X(t - d_O^k) + \sum_{j=1}^{n_I} \int_{t-h_j^k}^t e^{A(t-s-h_j^m)} B_j u_j(s) ds \quad (5.14)$$

and by multiplying both sides from left by $C_k e^{Ad_O^{mk}}$, one may write

$$C_k e^{Ad_O^{mk}} Z(t) = C_k X(t - d_O^k) + C_k W_k(t) \quad (5.15)$$

Now, substituting $C_k X(t - d_O^k)$ from (5.5) yields

$$C_k e^{Ad_O^{mk}} Z(t) = y_k^d(t) - \sum_{j=1}^{n_I} D_{kj} u_j(t - h_j^k) - H_k w(t - d_O^k) - v_k(t - d_O^k) + C_k W_k(t) \quad (5.16)$$

A new output vector for the k 'th channel, $y_z^k(t)$, is defined as

$$y_z^k(t) = C_k e^{Ad_O^{mk}} Z(t) + H_k w(t - d_O^k) + v_k(t - d_O^k) \quad (5.17)$$

or equivalently,

$$y_z(t) = C_z Z(t) + H_z w_z(t) + v_z(t) \quad (5.18)$$

with

$$C_z = \begin{bmatrix} C_1 e^{A d_o^{m_1}} \\ C_2 e^{A d_o^{m_2}} \\ \vdots \\ C_{n_o} e^{A d_o^{m_{n_o}}} \end{bmatrix} \quad (5.19)$$

and $w_z(t) = \left[w(t - d_o^1)^T \ \cdots \ w(t - d_o^{n_o})^T \right]^T$, $v_z(t) = \left[v(t - d_o^1)^T \ \cdots \ v(t - d_o^{n_o})^T \right]^T$,
 $H_z = \text{diag}\{H_k\}$.

Using (5.16), the reduced system outputs can be calculated from the delayed outputs (5.17) and W 's using

$$y_z^k(t) = y_k^d(t) - \sum_{j=1}^{n_I} D_{kj} u_j(t - h_j^k) + C_k W_k(t) \quad (5.20)$$

This completes the derivation of the reduced system dynamics and the output equations in (5.9) and (5.18). The calculation of the new observation vectors in (5.20) involves the computation of $W_k(t)$'s in (5.8) which are outputs of systems with finite impulse response (FIR). A less computationally expensive alternative to (5.8) suitable for real-time implementation can be obtained by differentiating (5.8)

$$\dot{W}_k(t) = A W_k(t) + \sum_{j=1}^{n_I} e^{-A h_j^k} B_j u_j(t) - \sum_{j=1}^{n_I} B_j u_j(t - h_j^k) \quad (5.21)$$

$$y_k^w(t) = C_k W_k(t) \quad (5.22)$$

It should be noted that since the states of the system are not directly available, an observer/controller pair should be designed to control the reduced system based on the new measurements. The following theorem is needed for the control of the reduced system.

Theorem 5.1: The reduced system in (5.9) and (5.18) is stabilizable and detectable if the original system in (5.1) and (5.2) is stabilizable and detectable.

Proof: see the appendix A.

Theorem 5.2: If the reduced delay-free system is stabilized through an observer/controller pair, the original delayed system will also become stable.

Proof: Since the stabilizability and detectability of the original system is preserved by the reduced delay-free system, an observer/controller (e.g. LQG controller) can be used to stabilize the reduced system. Such a controller guarantees that the reduced states $Z(t)$ and their estimates $\hat{Z}(t)$ remain bounded in the presence of bounded disturbance and noise. The control signal $u(t)$ is given by

$$u(t) = -K\hat{Z}(t) \quad (5.23)$$

where $\hat{Z}(t)$ is the observed states of the reduced system. This implies that the control signal is also bounded. From (5.7), the original system states can be written as

$$X(t - d_O^m) = Z(t) - W_m(t) \quad (5.24)$$

where

$$W_m(t) = \sum_{j=1}^{n_I} \int_{t-h_j^m}^t e^{A(t-s-h_j^m)} B_j u_j(s) ds \quad (5.25)$$

and $W_m(t)$ is bounded as a result of a bounded $u(t)$. Since both terms on the right hand side of (5.24) are bounded, $X(t - d^m)$ and consequently $X(t)$ are also bounded. Therefore the state observer/controller for the delay-free reduced system stabilizes the original system as well. Note that if zero is an asymptotically stable point for the reduced states $Z(t)$, then it would be also an asymptotically stable point for the original states $X(t)$. Q.E.D.

5.3 LQG Teleoperation Control

As shown in (3.4)-(3.5), the combined operator/master dynamics can be written as

$$\dot{X}_m(t) = A_m X_m(t) + B_m f_{cm}(t) + G_m w_m(t) \quad (5.26)$$

$$y_m(t) = C_m X_m(t) + D_m f_{cm}(t) + H_m w_m(t) + v_m(t) \quad (5.27)$$

where $X_m(t) = \begin{bmatrix} x_m(t) & v_m(t) \end{bmatrix}^T$ is the state vector and $y_m(t) = \begin{bmatrix} x_m(t) & f_h(t) \end{bmatrix}^T$ is the output vector. The control signal $f_{cm}(t)$ has been introduced in (3.1) and the disturbance signal is $w_m(t) = \begin{bmatrix} f_h^*(t) & \tilde{f}_{cm}(t) \end{bmatrix}^T$ where $\tilde{f}_{cm}(t)$ is the disturbance in the control signal $f_{cm}(t)$; $v_m(t)$ is measurement noise vector.

Similarly using (3.10)-(3.16), the slave/environment dynamics and the measurement equations can be written as

$$\dot{X}_s^i(t) = A_s^i X_s^i(t) + B_s^i f_{cs}(t) + G_s^i w_s(t) \quad i = 1, 2, 3 \quad (5.28)$$

$$y_s^i(t) = C_s^i X_s^i(t) + D_s^i f_{cs}(t) + H_s^i w_s(t) + v_s(t) \quad (5.29)$$

where indices 1, 2, 3 correspond to free motion, contact with a flexible environment, and contact with a rigid environment, respectively; $X_s^{1,2,3}(t) = \begin{bmatrix} x_s(t) & v_s(t) \end{bmatrix}^T$; $y_s(t) = \begin{bmatrix} x_s(t) & f_e(t) \end{bmatrix}$ is the measurement vector. The control signal is $f_{cs}(t)$ and the disturbance vector is $w_s(t) = \begin{bmatrix} f_e^*(t) & \tilde{f}_{cs}(t) \end{bmatrix}^T$. Note that the state transition matrices are function of the contact state i . The desired tool dynamics in (4.3) can also be written as

$$\dot{X}_t(t) = A_t X_t(t) + B_t u_t(t) \quad (5.30)$$

$$y_t(t) = X_t(t) \quad (5.31)$$

where $X_t(t) = \begin{bmatrix} x_t(t) & v_t(t) \end{bmatrix}^T$, $u_t(t) = \begin{bmatrix} f_h(t) & f_e(t) \end{bmatrix}^T$ and $y_t(t) = X_t(t)$.

Similar to the last chapter, the change in the environment parameters can be handled with a multi-model control approach proposed in chapter 3. Controllers are designed for each phase of the operation. Switching between these controllers occurs according to the estimated contact state.

5.3.1 Free motion/soft contact

The states of the system for the cases of free motion/soft contact are defined as follows

$$X(t) = \begin{bmatrix} \alpha_p X_s(t) - X_m(t) & X_m(t) - X_t(t) & X_t(t) \end{bmatrix}^T \quad (5.32)$$

where $X_m(t)$, $X_s(t)$, and $X_t(t)$ have been introduced in (5.26), (5.28) and (5.30); α_f and α_p have been defined in (4.3) and (4.4). The states evolution is governed by

$$\dot{X}(t) = AX(t) + Bu(t) + Gw(t) \quad (5.33)$$

and

$$u(t) = \begin{bmatrix} f_{cm}(t) & f_{cs}(t-d) \end{bmatrix}^T \quad (5.34)$$

$$w(t) = \begin{bmatrix} f_h^*(t) & f_e^*(t) & \tilde{f}_{cm}(t) & \tilde{f}_{cs}(t) \end{bmatrix}^T \quad (5.35)$$

A , B , G are calculated from A_m , B_m , C_m , D_m , G_m , H_m , A_s , B_s , C_s , D_s , G_s , H_s , A_t , and B_t . The measurement vector is

$$y(t) = \begin{bmatrix} y_m(t) & y_s(t-d) & y_t(t-d) \end{bmatrix}^T \quad (5.36)$$

where $y_m(t)$, $y_s(t)$, and $y_t(t)$ are defined in equations (5.27), (5.29), and (5.31) respectively.

Similar to the previous chapter, the operator's exogenous force $f_h^*(t)$ is modelled by a stochastic process and added to the system states. A second-order model

with a pair of repeated poles at $-\alpha_{fh}$ is used, i.e.

$$\ddot{f}_h^*(t) + 2\alpha_{fh}\dot{f}_h^*(t) + \alpha_{fh}^2 f_h^*(t) = n_f(t) \quad (5.37)$$

where $n_f(t)$ is white Gaussian noise. The state-space equations of the system in free motion/soft contact after the augmentation of f_h^* into the state vector are given by

$$\dot{X}_f(t) = A_f X_f(t) + B_f u_f(t) + G_f w_f(t) \quad (5.38)$$

$$y_f(t) = C_f X_f(t) + H_f w_f(t) + v_f(t) \quad (5.39)$$

and

$$X_f(t) = \begin{bmatrix} X(t) & f_h^*(t) & \dot{f}_h^*(t) \end{bmatrix}^T \quad (5.40)$$

$$y_f(t) = y(t) = \begin{bmatrix} y_m(t) & y_s(t-d) & y_t(t-d) \end{bmatrix}^T \quad (5.41)$$

$$u_f(t) = u(t) = \begin{bmatrix} f_{cm}(t) & f_{cs}(t-d) \end{bmatrix}^T \quad (5.42)$$

$$w_f(t) = \begin{bmatrix} n_f(t) & f_e^*(t) & \tilde{f}_{cm}(t) & \tilde{f}_{cs}(t) \end{bmatrix}^T \quad (5.43)$$

$$v_f(t) = \begin{bmatrix} v_m(t) & v_s(t) & 0 \end{bmatrix}^T \quad (5.44)$$

There is a d second delay for the slave measurements to reach the controller and for the control signal to arrive at the slave. Also, the virtual tool states are available to the controller with the same amount of time lag. Assuming that the master, slave, and tool measurements are 1st, 2nd, 3rd output channels and master

and slave control signals are 1st, 2nd input channels, respectively, one may write

$$d_I^1 = d_O^1 = 0$$

$$d_I^2 = d_O^2 = d$$

$$d_O^3 = d$$

Since the maximum output delay d_O^m is d ,

$$h_1^m = d, \quad h_2^m = 2d \quad (5.45)$$

After the application of the transformation in (5.7), the reduced system dynamics in free motion/soft contact are governed by the following equations

$$\dot{Z}_f(t) = A_{zf}Z_f(t) + B_{zf}u_z(t) + G_{zf}w_f(t - d_O^m) \quad (5.46)$$

with

$$A_{zf} = A_f \quad (5.47)$$

$$B_{zf} = \begin{bmatrix} e^{-A_f d} B_f^1 & e^{-2A_f d} B_f^2 \end{bmatrix}^T \quad (5.48)$$

$$G_{zf} = G_f \quad (5.49)$$

where B_f^1 and B_f^2 are the first and second columns of B_f , respectively; $u_z(t)$ is a delay-free variation of the control vector $u(t)$ in (5.34). The output equation of the

reduced system is as follows

$$y_{zf}(t) = C_{zf}Z_f(t) + H_{zf}w_{zf}(t) + v_{zf}(t) \quad (5.50)$$

where

$$C_{zf} = \begin{bmatrix} C_f^1 e^{A_f d} \\ C_f^2 \\ C_f^3 \end{bmatrix} \quad (5.51)$$

$$H_{zf} = H_f \quad (5.52)$$

with C_f^1 , C_f^2 and C_f^3 being the rows of C_f corresponding to the master, slave and tool measurements, respectively.

5.3.2 Rigid contact

When the slave is in rigid contact, its dynamics are governed by (3.12)-(3.14). The vector of states is chosen as

$$X(t) = [x_m(t) - \alpha_p x_s(t) \quad v_m(t) \quad x_s(t) \quad \tilde{f}_e(t) \quad \alpha_f \tilde{f}_e(t) - \tilde{f}_h(t)]^T \quad (5.53)$$

and the measurement vector is

$$y(t) = \begin{bmatrix} y_m(t) & x_s(t-d) & \tilde{f}_e(t-d) \end{bmatrix}^T \quad (5.54)$$

In (5.53), $\tilde{f}_e(t)$ and $\tilde{f}_h(t)$ are generated by passing force sensor measurements $f_e(t)$ and $f_h(t)$ through the following first-order filters with poles at $-\beta$

$$\dot{\tilde{f}}_e(t) + \beta\tilde{f}_e(t) = \beta f_{cs} \quad (5.55)$$

$$\dot{\tilde{f}}_h(t) + \beta\tilde{f}_h(t) = \beta f_h \quad (5.56)$$

The reason for adding \tilde{f}_e to the states is that the model of rigid contact in (3.12)-(3.14) only involves some algebraic constraints. The first-order filters introduce new states for the slave and enable the application of the LQG control synthesis. The dynamics of filtered force tracking error $\alpha_f \tilde{f}_e - \tilde{f}_h$ can be easily derived from the filter equations above,

$$\alpha_f \dot{\tilde{f}}_e(t) - \dot{\tilde{f}}_h(t) = -\beta(\alpha_f \tilde{f}_e(t) - \tilde{f}_h(t)) + \alpha_f \beta f_{cs} - \beta f_h \quad (5.57)$$

and f_h can be written in terms of the states and inputs. The slave position in rigid contact $x_s(t)$ is modelled by

$$\dot{x}_s(t) = w_{xs}(t) \quad (5.58)$$

where $w_{xs}(t)$ is a small white Gaussian noise. The steps for incorporating the operator's exogenous force $f_h^*(t)$ into the system's states are similar to those in the

previous case and will not be repeated here. The dynamics of the augmented system can be expressed by the following equation

$$\dot{X}_r(t) = A_r X_r(t) + B_r u_r(t) + G_r w_r(t) \quad (5.59)$$

$$y_r(t) = C_r X_r(t) + D_r u_r(t) + H_r w_r(t) + v_r(t) \quad (5.60)$$

with

$$X_r(t) = \begin{bmatrix} X(t) & f_h^*(t) & \dot{f}_h^*(t) \end{bmatrix}^T \quad (5.61)$$

$$y_r(t) = y(t) = \begin{bmatrix} y_m(t) & y_s(t-d) & \tilde{f}_e(t-d) \end{bmatrix} \quad (5.62)$$

$$u_r(t) = \begin{bmatrix} f_{cm}(t) & f_{cs}(t-d) \end{bmatrix}^T \quad (5.63)$$

$$w_r(t) = \begin{bmatrix} n_f(t) & \tilde{f}_{cm}(t) & \tilde{f}_{cs}(t) & w_{xs}(t) \end{bmatrix} \quad (5.64)$$

$$v_r(t) = \begin{bmatrix} v_m(t) & 0 \end{bmatrix} \quad (5.65)$$

It should be noted that the virtual tool dynamics are not used in the rigid contact controller. Assuming that master and slave inputs and outputs are the first and second channels, respectively, one can write

$$d_I^1 = d_O^1 = 0$$

$$d_I^2 = d_O^2 = d$$

The maximum output delay d_O^m is d . So,

$$h_1^m = d$$

$$h_2^m = 2d$$

Dynamics of the reduced system are governed by the followings equations

$$\dot{Z}_r(t) = A_{zr}Z_r(t) + B_{zr}u_z(t) + G_{zr}w_r(t - d_O^m) \quad (5.66)$$

where

$$A_{zr} = A_r \quad (5.67)$$

$$B_{zr} = \begin{bmatrix} e^{-dA_r} B_r^1 & e^{-2dA_r} B_r^2 \end{bmatrix}^T \quad (5.68)$$

$$G_{zr} = G_r \quad (5.69)$$

and B_r^1 and B_r^2 are the first and second columns of B_r , respectively; u_z is the new delay-free control vector. The output equations of the reduced system are as follows

$$y_{zr}(t) = C_{zr}Z_r(t) + H_{zr}w_{zr}(t) + v_{zr}() \quad (5.70)$$

where

$$C_{zr} = \begin{bmatrix} C_r^1 e^{dA_r} \\ C_r^2 \end{bmatrix} \quad (5.71)$$

$$H_{zr} = H_r \quad (5.72)$$

5.3.3 LQG control synthesis

The system dynamics equations in (5.46)-(5.52) for free motion/soft contact and in (5.66)-(5.72) for rigid contact are suitable for the application of the LQG control synthesis. The LQG controller will minimize the following loss function as $T \rightarrow \infty$ [89]

$$J(u) = \frac{1}{T} E \left\{ \int_0^T (Z(t)^T Q Z(t) + u_z(t)^T R u_z(t)) dt \right\} \quad (5.73)$$

where $E\{\cdot\}$ denotes the expected value, and $Q \geq 0, R > 0$. The controller is a state feedback gain combined with a *Kalman* filter state estimator, i.e.

$$u(t) = -K \hat{Z}(t) \quad (5.74)$$

where K is given by

$$K = R^{-1} B^T S \quad (5.75)$$

and S is the solution to the following *Continuous-time Algebraic Riccati Equation* (CARE)

$$A^T S + S A - S B R^{-1} B^T S + Q = 0 \quad (5.76)$$

The state estimate $\hat{X}(t)$ is the output of a *Kalman* filter with the following dynamics

$$\dot{\hat{Z}}(t) = A \hat{Z}(t) + B u_z(t) + L (y_z(t) - C \hat{Z}(t) - D u(t)) \quad (5.77)$$

The *Kalman* filter gain L is computed as follows [89]

$$L = PC^T\Pi^{-1} \quad (5.78)$$

where P is the solution to the following CARE

$$PA^T - PC^T\Pi^{-1}CP + AP + W = 0 \quad (5.79)$$

with $W = E\{Gw(t)w(t)^TG^T\}$ and $\Pi = E\{v(t)v(t)^T\}$ being the covariances of the process and measurement noise, respectively. Stabilizability of pair (A, B) and detectability of pair (C, A) are required for the existence of a solution to the LQG problem. It can be shown that the a teleoperation system has all the necessary conditions. Furthermore in Theorem 3.1, it was proven that the stabilizability and detectability are preserved under the proposed state and output transformations.

For free motion/soft contact, one may write:

$$X_f(t)^T Q_f X_f(t) = q_1(\alpha_p x_s(t) - x_m(t))^2 + q_2(x_m(t) - x_t(t))^2 \quad (5.80)$$

with $q_1 > 0$ and $q_2 > 0$. Similarly for rigid contact,

$$X_r(t)^T Q_r X_r(t) = q_1(x_m(t) - \alpha_p x_s(t))^2 + q_2(\alpha_f \tilde{f}_e(t) - \tilde{f}_h(t))^2 \quad (5.81)$$

It should be noted that the LQG control synthesis in (5.73) is conducted using the transformed states $Z(t)$ rather than the original states. Proper scaling for matrices Q_f and Q_r may be obtained by considering the approximation $Z(t) \approx e^{A_{d\tilde{O}} t} X(t) -$

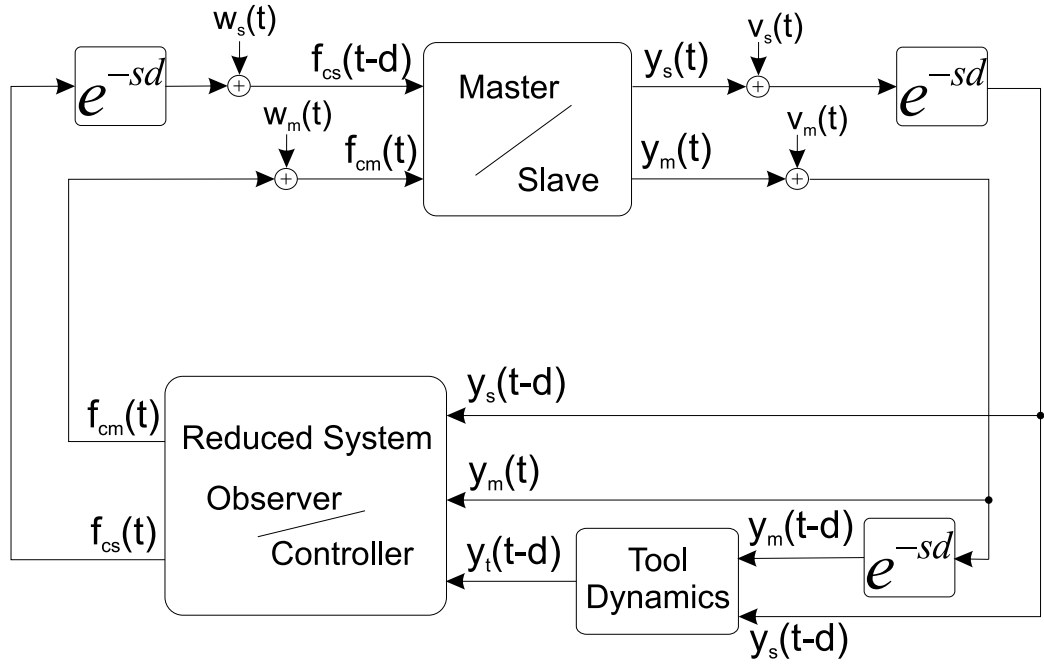


Figure 5.2: The system architecture when teleoperation controller resides at the master side.

d_O^m); therefore,

$$Z(t)^T Q_z Z(t) \approx X(t - d_O^m)^T e^{A^T d_O^m} Q e^{A d_O^m} X(t - d_O^m) \quad (5.82)$$

The schematic of the proposed LQG teleoperation controller is depicted in Figure 5.2.

5.4 Simulation Results

The same single-axis bilateral teleoperation system is used here as well (see figure 3.3). The controller is again implemented at the master side. Two different controllers are designed for two phases of operation, i.e. free motion and contact

with rigid environments. The system and tool parameters are the same as those mentioned in chapters 3 and 4 (see (3.29) and (4.64)), with the addition of the following parameters.

Additional system parameters:

$$\alpha_f = 1 \quad \alpha_p = 1 \quad \alpha_{fh} = 0.01$$

LQG parameters for free motion controller:

$$q_1 = q_2 = 10^6$$

$$R = \text{diag}(0.1, 0.1)$$

$$E\{w_f w_f^T\} = \text{diag}(10^4, 200, 10^{-3}, 10^{-3}, 10^4, 200, 10^{-3}, 10^{-3})$$

$$E\{v_f v_f^T\} = \text{diag}(10^{-10}, 10^{-5}, 10^{-10}, 10^{-5}, 10^{-9}, 10^{-4})$$

LQG parameters for rigid contact:

$$q_1 = 10^5, \quad q_2 = 100$$

$$R = \text{diag}(0.01, 0.01)$$

$$\beta = 0.8$$

$$E\{w_r w_r^T\} = \text{diag}(1, 10^{-6}, 10^{-6}, 10^{-5})$$

$$E\{v_r v_r^T\} = \text{diag}(10^{-9}, 10^{-4}, 10^{-9}, 10^{-4})$$

Same as previous chapter, various simulation scenarios are considered, i.e. under different communication delays with matched and mismatched parameters.

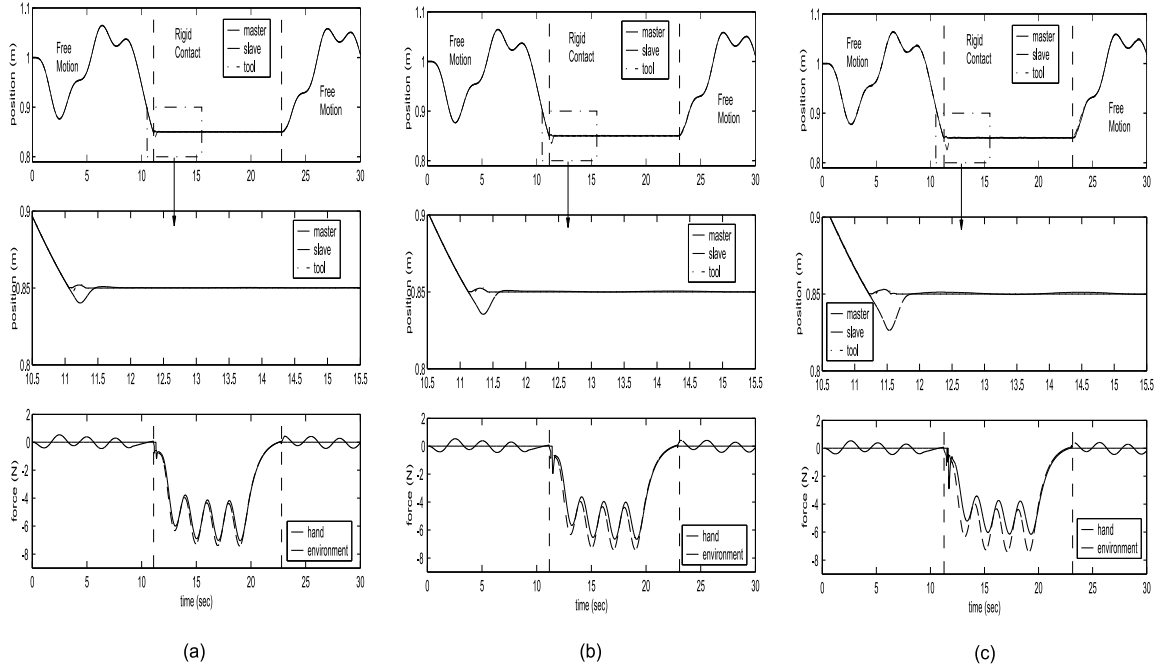


Figure 5.3: Position and force tracking in simulation for matched parameters: (a) 125ms delay (b) 250ms delay (c) 500ms delay.

(i) Simulations with matched parameters:

Levels of round-trip time-delay are chosen to be similar to the ones in chapter 4, i.e. 125ms, 250ms, and 500ms. Figure 5.3 shows excellent position and force tracking as well as impedance shaping in free motion. The controller also demonstrates a stable behavior both in contact phase and in free motion/rigid contact transitions.

(ii) Simulations with mismatched parameters:

Figure 5.4 presents the simulation results for the case of mismatched parameters, i.e. $m_h(\text{real}) = 1\text{kg}$ and $m_h(\text{model}) = 0.35\text{kg}$. The controller still demonstrates stable force and position tracking with a high performance. Responses were also quite satisfactory for all levels of delays in case of $m_h(\text{real}) = 0.05\text{kg}$.

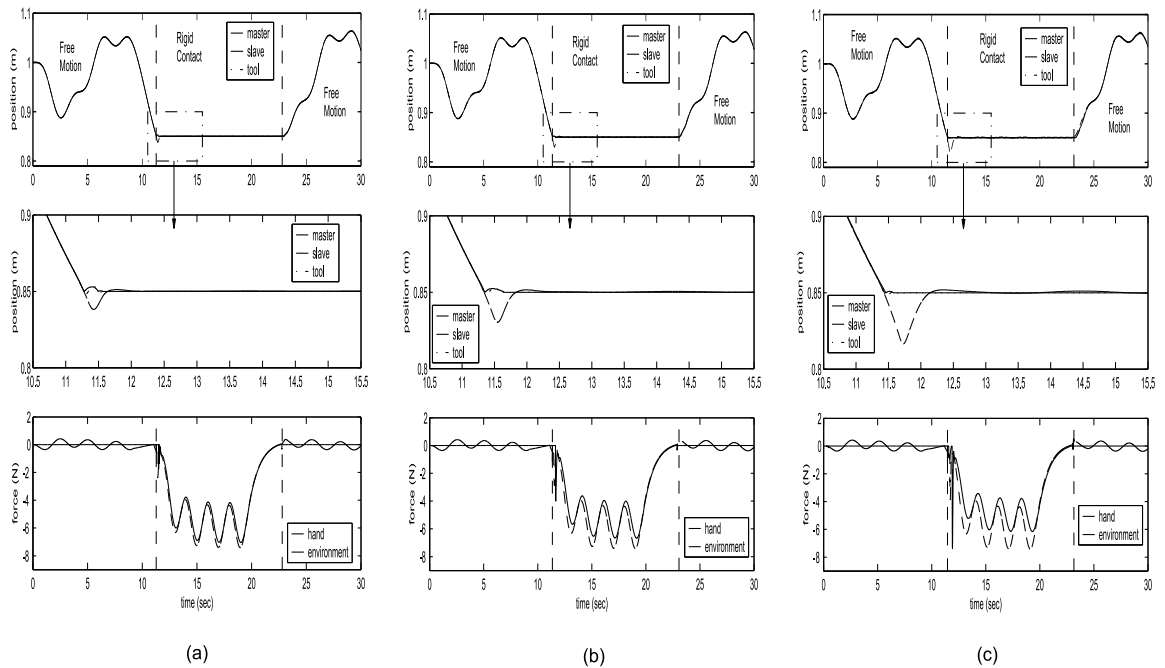


Figure 5.4: Position and force tracking in simulation for mismatched model parameters: (a) 125ms delay (b) 250ms delay (c) 500ms delay.

5.5 Experimental Results

The single-axis experimental setup depicted in figure 3.6 is again used in experiments with the sampling frequency of 1024 Hz which is higher than 256 Hz, the sampling time used in discrete-time LQG controller. As mentioned before, higher sampling rates can be employed for the continuous-time LQG controller compared with discrete-time controller and this is because of the fact that unlike continuous-time controller, delayed inputs and outputs are inserted in the state vector in the discrete-time method. The experiments were conducted for three different round-trip time delays, i.e. 63ms, 125ms, and 250ms.

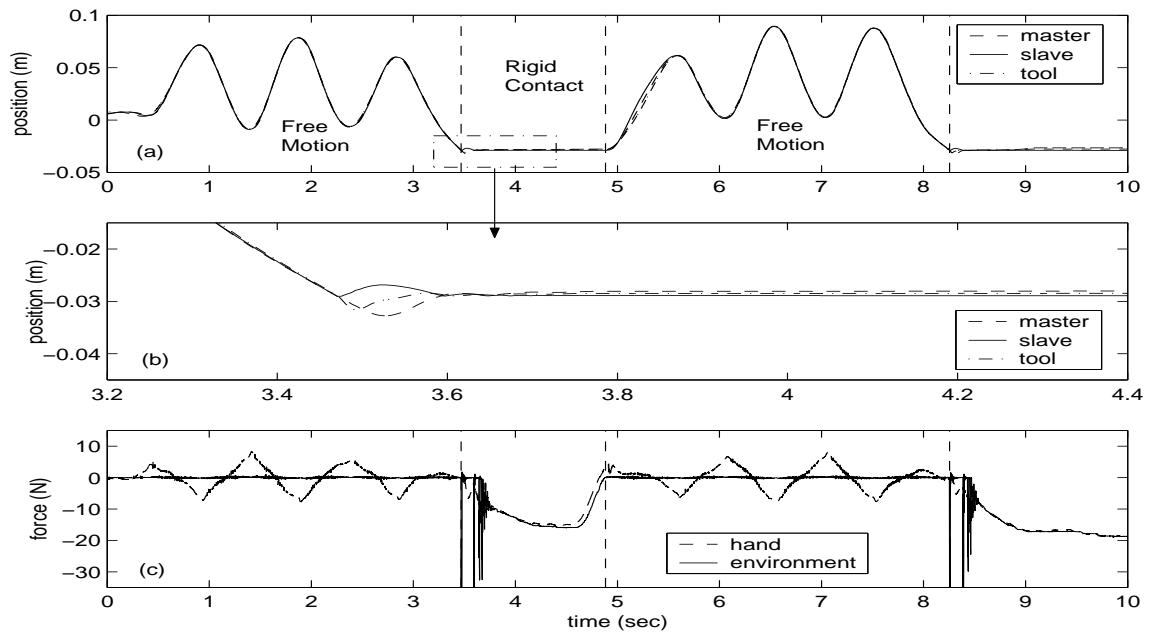


Figure 5.5: LQG controller with 63ms delay in experiment: (a) position tracking for master/slave/virtual tool; (b) contact transition (c) force tracking.

5.5.1 LQG controller with 63ms delay

Figure 5.5, illustrates the results of the proposed controller for 63ms delay in communication channel. Performance objectives, such as position and force tracking and impedance shaping are fully satisfied while the controller provides stable contact and free motion/rigid contact transitions.

Same as in previous cases, there is a small position tracking error for master device just after hitting the rigid wall, which depends on the amount of time-delay.

5.5.2 LQG controller with 125ms delay

Figure 5.6 presents the results for round-trip time-delay of 63ms. The controller shows an acceptable position tracking in free motion as well as force tracking in

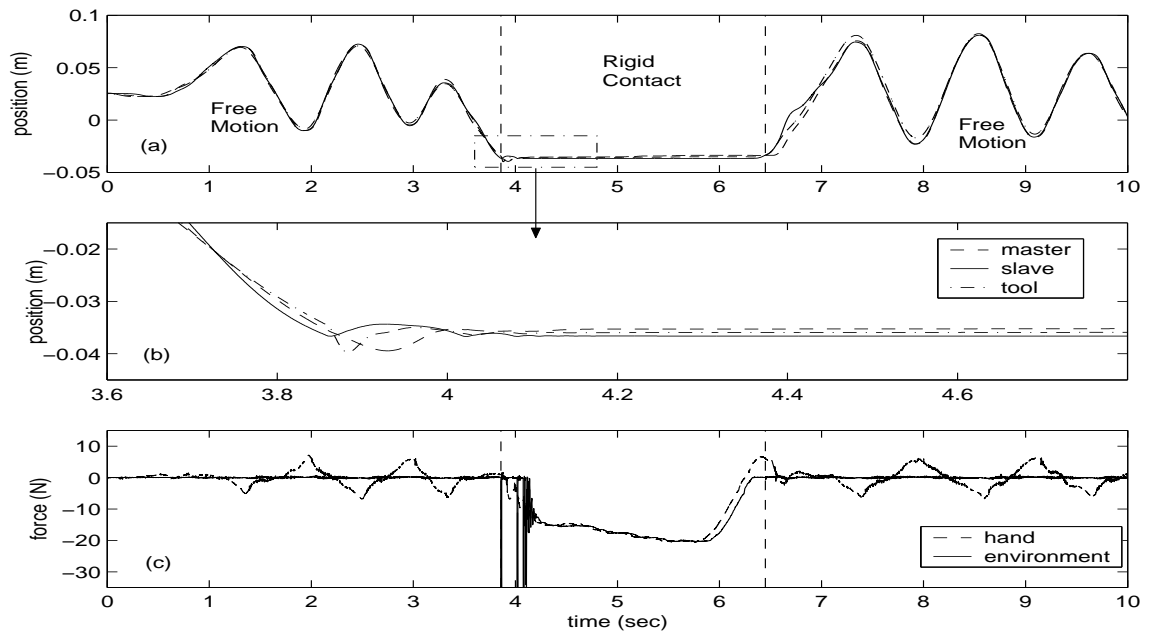


Figure 5.6: LQG controller with 125ms delay in experiment: (a) position tracking for master/slave/virtual tool; (b) contact transition (c) force tracking.

rigid contact.

5.5.3 LQG controller with 250ms delay

The results of the experiment with 250 ms delay is shown in Figure 5.7. The controller provides a quite satisfactory response, while there is a slight degradation in the performance of the free motion tracking.

Again, the position and force tracking results can be compared with those of the two-channel controller (depicted in Figure 4.11). Clearly from these figures, the continuous-time reduction method and LQG controller outperform the traditional two-channel teleoperation controller in presence of time-delay.

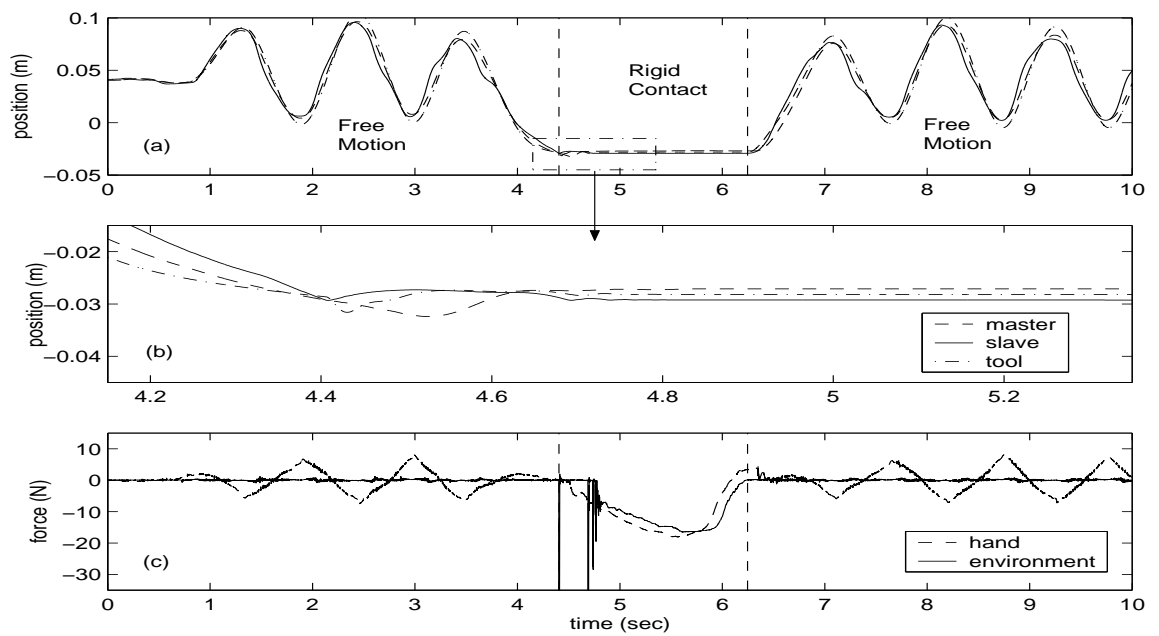


Figure 5.7: LQG controller with 250ms delay in experiment: (a) position tracking for master/slave/virtual tool; (b) contact transition (c) force tracking.

Chapter 6

Conclusions and Future Work

Most existing teleoperation control techniques sacrifice transparency objectives in order to gain robust stability in the presence of environment uncertainties and communication delay between the master and slave sites. With the aim of achieving a transparent response, we studied these two problems.

To deal with environment changes, an adaptive method for teleoperation was introduced. Multiple models describe dynamic behavior of the slave in free motion and in contact with rigid environments. A multiple-model state estimation technique calculates the mode probabilities based on the available sensory information. The control action is computed by combining the mode-based control signals according to the mode probabilities. Simulation and experimental studies demonstrated the superiority of the proposed adaptive controller over a fixed-gain four-channel teleoperation controller.

The treatment of delay problem in the discrete-time domain allowed for the inclusion of the delay in the measurement and control signals into the system

state space model. Teleoperation performance objectives such as non-delayed virtual tool impedance shaping, position tracking, and force tracking were achieved through the application of the LQG control synthesis. Different controllers were designed for free motion/soft contact and contact with rigid environments. Switching between the controllers occur according to the identified mode of operation. The Nyquist technique was utilized to analyze the robustness of the controller with respect to variations in the system's parameters. Simulation and experimental studies with a single-axis teleoperation system demonstrated that the proposed approach is highly successful in providing stable and transparent response under communication delay when compared with a two-channel position-position controller.

A reduction method was proposed in this manuscript to transform a dynamical system with delays in control actions and measurements to a system without delay. An LQG controller was then designed and employed for the reduced system. The same performance objectives, i.e. position and force tracking as well as virtual tool impedance shaping, were obtained through LQG controller design. Simulation and experimental studies showed that the proposed method easily outperforms traditional teleoperation methods in providing the operator with a transparent and stable interface.

In order to operate under large delays, based on our experience, a good knowledge of the model parameters is required. This might have been expected as the proposed method is essentially a model-based predictive controller. In general, it is hard to find a meaningful bound on the time delay that our approach can handle as such limit would depend on various factors such as the system dynamics, the

required level of performance, and the amount of uncertainty in the parameters. The experimental results indicated that an excellent performance with good stability margins can be obtained under delays of up to 200 – 300ms in our experimental setup. To move beyond this level, the performance has to be sacrificed in favor of the robust stability of the system.

As a future work, the controller can be modified to develop an adaptive variation, which can cope with parametric uncertainties and improve the robustness of the system under longer communication delays. Also, a variation of the method which can handle variable time delays can be developed.

Appendix A

Proof of Theorem 5.1

A.1 Stabilizability

The controllability matrix of the original system with pair (A, B) can be written as

$$U = [B \ AB \ A^2B \ \cdots \ A^{n-1}B] = [B_1 \ \cdots \ B_{n_I} | AB_1 \ \cdots \ AB_{n_I} | \cdots | A^{n-1}B_1 \ \cdots \ A^{n-1}B_{n_I}] \quad (\text{A.1})$$

where the rank of U is

$$\rho(U) = n_c \leq n \quad (\text{A.2})$$

Using the canonical decomposition theorem [88], there exists a transformation $\bar{X} = PX$, which transforms pair (A, B) to (\bar{A}, \bar{B})

$$\bar{A} = PAP^{-1} = \begin{bmatrix} \bar{A}^c & \bar{A}^{12} \\ 0 & \bar{A}^e \end{bmatrix} \quad (\text{A.3})$$

$$\bar{B} = PB = \begin{bmatrix} \bar{B}^c \\ 0 \end{bmatrix} \quad (\text{A.4})$$

such that the pair (\bar{A}^c, \bar{B}^c) is controllable. The state transformation matrix P is defined as

$$P^{-1} \triangleq Q = [q_1 \cdots q_{n_c} \cdots q_n] \quad (\text{A.5})$$

where $q_1 \cdots q_{n_c}$ are n_c linearly independent columns of matrix U and the last $n - n_c$ columns are arbitrarily chosen vectors that make the matrix Q nonsingular. Since the original system is assumed stabilizable, \bar{A}^c would contain all unstable modes, if any.

From (5.9), the controllability matrix of the transformed system represented by the pair (A_z, B_z) is given by

$$U_z = [B_z \ A_z B_z \ A_z^2 B_z \ \cdots \ A_z^{n-1} B_z] = \\ [e^{-Ah_1^m} B_1 \ \cdots \ e^{-Ah_{n_I}^m} B_{n_I} | e^{-Ah_1^m} A B_1 \ \cdots \ e^{-Ah_{n_I}^m} A B_{n_I} | \cdots \\ | e^{-Ah_1^m} A^{n-1} B_1 \ \cdots \ e^{-Ah_{n_I}^m} A^{n-1} B_{n_I}] \quad (\text{A.6})$$

where the commutability of matrices A and e^{-Ah} has been used. The following lemma is needed to continue the proof.

Lemma A.1:

$$\rho(U_z) = \rho(U) \quad (\text{A.7})$$

Proof: Reordering the columns of a matrix will not alter its rank, so from (A.6)

$$\rho(U_z) = \rho([e^{-Ah_1^m} [B_1 \ AB_1 \ \cdots \ A^{n-1}B_1] \ | \ \cdots \ | e^{-Ah_{n_I}^m} [B_{n_I} \ AB_{n_I} \ \cdots \ A^{n-1}B_{n_I}]]) \quad (\text{A.8})$$

Note that since $e^{-Ah_j^m}$ is a full rank square matrix, for each j ,

$$\rho([e^{-Ah_j^m} [B_j \ AB_j \ \cdots \ A^{n_I-1}B_j]]) = \rho([B_j \ AB_j \ \cdots \ A^{n_I-1}B_j]) \quad (\text{A.9})$$

To proceed, we use the *Caley-Hamilton* theorem which states that each matrix satisfies its own characteristic polynomial [88], i.e.

$$f(A) = a_n A^n + a_{n-1} A^{n-1} + \cdots + a_0 = 0 \quad (\text{A.10})$$

and therefore,

$$A^n = b_{n-1} A^{n-1} + \cdots + b_0 \quad (\text{A.11})$$

and consequently, all the powers of A greater than or equal to n can be written as

a linear combination of A^k , for $k < n$. Using this theorem and the *Taylor* series expansion of $e^{-Ah_j^m}$, one can write

$$e^{-Ah_j^m} = c_0I + c_1A + c_2A^2 + \dots + c_{n-1}A^{n-1} \quad (\text{A.12})$$

Using (A.12),

$$\begin{aligned} e^{-Ah_j^m} A^k B_j &= (c_0I + c_1A + c_2A^2 + \dots + c_{n-1}A^{n-1})A^k B_j \\ &= l_0B_j + l_1AB_j + l_2A^2B_j + \dots + l_{n-1}A^{n-1}B_j \end{aligned} \quad (\text{A.13})$$

Considering (A.9) and (A.13), one can conclude that for each j , $[B_j \ AB_j \ \dots \ A^{n-1}B_j]$ and $e^{-Ah_j^m} [B_j \ AB_j \ \dots \ A^{n-1}B_j]$ span the same space. Therefore, U and U_z are of the same rank and the proof of Lemma A.1 is complete. Q.E.D.

The canonical form of the reduced system represented by the pair (\bar{A}_z, \bar{B}_z) can be generated using the same transformation P in (A.5) for the original system, i.e.

$$\bar{A}_z = PA_zP^{-1} \quad (\text{A.14})$$

$$\bar{B}_z = PB_z \text{ or } P^{-1}\bar{B}_z = B_z \quad (\text{A.15})$$

Substituting A_z and B_z from (5.10) and (5.11), results in

$$\bar{A}_z = PAP^{-1} = \begin{bmatrix} \bar{A}^c & \bar{A}^{12} \\ 0 & \bar{A}^{\bar{c}} \end{bmatrix} \quad (\text{A.16})$$

$$P^{-1} [\bar{b}_z^1 \dots \bar{b}_z^{n_I}] = [e^{-Ah_1^m} B_1 \dots e^{-Ah_{n_I}^m} B_{n_I}] \quad (\text{A.17})$$

For the j th column of (A.17), one can write

$$P^{-1} \bar{b}_z^j = e^{-Ah_j^m} B_j \quad (\text{A.18})$$

Replacing $e^{-Ah_j^m}$ from (A.12)

$$P^{-1} \bar{b}_z^j = (c_0 I + c_1 A + c_2 A^2 + \dots + c_{n-1} A^{n-1}) B_j \quad (\text{A.19})$$

From the definition of P^{-1} in (A.5), the first n_c columns of P^{-1} are the basis of the controllability matrix U in (A.1). Considering (A.19), the right hand side of (A.17) can be written in terms of first n_c columns of P^{-1} , i.e.

$$\bar{B}_z = \begin{bmatrix} \bar{B}_z^c \} n_c \\ 0 \end{bmatrix} \quad (\text{A.20})$$

Using (A.16) and (A.20), the controllability matrix of the pair (\bar{A}_z, \bar{B}_z) can be written as

$$\bar{U}_z = \begin{bmatrix} \bar{B}_z^c & \bar{A}_c \bar{B}_z^c & \dots & \bar{A}_c^{n-1} \bar{B}_z^c \} n_c \\ 0 & 0 & \dots & 0 \end{bmatrix} \quad (\text{A.21})$$

According to Lemma A.1, $\rho(U_z) = \rho(U) = n_c$. Also, since the transformation P is nonsingular, U_z and \bar{U}_z have equal ranks, i.e.,

$$\rho(\bar{U}_z) = n_c \quad (\text{A.22})$$

and consequently, the pair (\bar{A}^c, \bar{B}_z^c) is controllable where \bar{A}^c contains all the unstable poles.

A.2 Detectability

The proof follows the same lines as in the case of stabilizability. The observability matrix of the original system (A, B) can be written as

$$V = \begin{bmatrix} C \\ CA \\ CA^2 \\ \vdots \\ CA^{n-1} \end{bmatrix} = \begin{bmatrix} C_1 \\ \vdots \\ C_{n_o} \\ \text{---} \\ C_1 A \\ \vdots \\ C_{n_o} A \\ \text{---} \\ \vdots \\ \text{---} \\ C_1 A^{n-1} \\ \vdots \\ C_{n_o} A^{n-1} \end{bmatrix} \quad (\text{A.23})$$

where the rank of V is

$$\rho(V) = n_{ob} \leq n \quad (\text{A.24})$$

Using the canonical decomposition theorem [88], there exists a transformation $\bar{X} = PX$, which transforms pair (A, C) to (\bar{A}, \bar{C})

$$\bar{A} = PAP^{-1} = \begin{bmatrix} \bar{A}^o & 0 \\ \bar{A}^{21} & \bar{A}^{\bar{o}} \end{bmatrix} \quad (\text{A.25})$$

$$\bar{C} = CP^{-1} = \begin{bmatrix} \bar{C}^o & 0 \end{bmatrix} \quad (\text{A.26})$$

and the pair (\bar{A}^o, \bar{C}^o) is observable. The matrix P is defined as

$$P \triangleq \begin{bmatrix} r_1 \\ \vdots \\ r_{n_o} \\ \vdots \\ r_n \end{bmatrix} \quad (\text{A.27})$$

where $r_1 \cdots r_{n_{ob}}$ are n_{ob} independent rows of V and the last $n - n_{ob}$ rows are arbitrarily chosen vectors such that the matrix P is nonsingular. The detectability of the original system requires all unstable modes to be observable. Therefore, \bar{A}^o should contain all unstable modes. The canonical representation of the reduced system (\bar{A}_z, \bar{C}_z) can be obtained using transformation P in (A.27) from the original system.

$$\bar{A}_z = PA_zP^{-1} \quad (\text{A.28})$$

$$\bar{C}_z = C_z P^{-1} \text{ or } \bar{C}_z P = C_z \quad (\text{A.29})$$

Substituting A_z and C_z from (5.9) and (5.18), results in

$$\bar{A}_z = P A P^{-1} = \begin{bmatrix} \bar{A}^o & 0 \\ \bar{A}^{21} & \bar{A}^{\bar{o}} \end{bmatrix} \quad (\text{A.30})$$

$$\begin{bmatrix} \bar{C}_z^1 \\ \vdots \\ \bar{C}_z^{n_o} \end{bmatrix} P = \begin{bmatrix} C_1 e^{Ad_o^{m_1}} \\ C_2 e^{Ad_o^{m_2}} \\ \vdots \\ C_{n_o} e^{Ad_o^{m_{n_o}}} \end{bmatrix} \quad (\text{A.31})$$

For the j th row of (A.31), one can write

$$\bar{C}_z^j P = C_j e^{Ad_o^{m_j}} \quad (\text{A.32})$$

Using the Caley-Hamilton theorem,

$$\bar{C}_z^j P = C_j (a_0 I + a_1 A + a_2 A^2 + \cdots + a_{n-1} A^{n-1}) \quad (\text{A.33})$$

From the definition of P in (A.27), the first n_{ob} rows of P are the basis of matrix V in (A.23). Therefore, the right hand side of (A.31) can be written in terms of the first n_{ob} rows of P , i.e.

$$\bar{C}_z = \begin{bmatrix} \bar{C}_z^o & 0 \end{bmatrix} \quad (\text{A.34})$$

Using (A.30) and (A.34), the observability matrix of the pair (\bar{A}_z, \bar{C}_z) can be written as

$$\bar{V}_z = \begin{bmatrix} \bar{C}_z^o & 0 \\ \bar{C}_z^o \bar{A}_o & 0 \\ \vdots & \\ \bar{C}_z^o \bar{A}_o^{n-1} & 0 \end{bmatrix} \quad (\text{A.35})$$

Using the dual arguments of Lemma A.1, $\rho(\bar{V}_z) = n_{ob}$, and hence the pair (\bar{A}^o, \bar{C}_z^o) is observable. Also from the canonical decomposition theorem, \bar{A}^o encompasses all unstable poles. Consequently, the reduced system is detectable. Q.E.D

Bibliography

- [1] T. Sheridan, "Telerobotics," *Automatica*, vol. 25, no. 4, pp. 487–507, 1989.
- [2] C. Melchiorri and A. Eusebi, "Telemanipulation: system aspects and control issues," in *Proc. Model. Cont. Mechan. Robot.*, pp. 149–183, 1996.
- [3] T. Sheridan, *Teletobotics, Automation, and Human Supervisory Control*. Cambridge, Massachusetts: The MIT Press, 1992.
- [4] T. Sheridan, "Space teleoperation through time delay: review and prognosis," *IEEE Trans. Robot. Automat.*, vol. 9, no. 5, pp. 592–606, 1993.
- [5] K. Landzettel, B. Brunner, A. Beyer, E. Kramer, and C. Preusche, "Rokviss verification of advanced telepresence concepts for future space missions," in *7th ESA Workshop on Advances Space Technologies for Robotics and Automation 'ASTRA2002'*, Noordwijk, Netherlands, 2002.
- [6] G. Hirzinger, G. Grunwald, B. Brunner, and J. Heindl, "A sensor-based telerobotics systems for the space robot experiment rotex," in *Proc. IEEE Int. Conf. Robot. Auto.*, 1992.
- [7] M. Oda, "Japan's space automation and robotics activities," in *Proc. IEEE Int. Conf. Robot. Auto.*, 1992.

- [8] C. Stoker, D. Barch, B. Hine, and J. Barry, "Antarctic undersea exploration using a robotic submarine with a telepresence user interface," *IEEE Expert*, vol. 10, no. 6, pp. 14–23, 1995.
- [9] D. Kwon, J. Ryu, P. Lee, and S. Hong, "Design of a teleoperation controller for an underwater manipulator," in *Proc. IEEE Int. Conf. Robot. Auto.*, 2000.
- [10] A. Kwitowski, W. Mayercheck, and A. Brautigam, "Teleoperation for continuous miners and haulage equipment," *IEEE Trans. Ind. Gen. Applicat.*, vol. 28, no. 5, pp. 1118–1125, 1992.
- [11] J. Park, K. Kim, H. Lee, and M. Yang, "Robotic contamination cleaning system," in *Proc. IEEE Conf. on Intelligent Robots and Systems*, 2002.
- [12] R. Taylor, "Medical robotics in computer-integrated surgery," *IEEE Trans. Robot. Automat.*, vol. 19, no. 5, pp. 765–781, 2003.
- [13] A. Madhani, G. Niemeyer, and J. Salisbury, "The black falcon: A teleoperated surgical instrument for minimally invasive surgery," in *Proc. IEEE Int. Conf. on Intelligent Robots and Systems*, 1998.
- [14] S. Salcudean, "Control for teleoperation and haptic interfaces," *Control Problems in Robotics and Automation LNCIS230*, B. Siciliano and K.P. Valavanis (Eds.). Springer, pp. 51–66, 1998.
- [15] D. Lawrence, "Stability and transparency in bilateral teleoperation," *IEEE Trans. Robot. Automat.*, vol. 9, pp. 624–637, October 1993.
- [16] K. Astrom and B. Wittenmark, *Computer-Controlled Systems: Theory and Design*, 3rd Edition. Prentice Hall, 1997.

- [17] R. Luck and A. Ray, "An observer-based compensator for distributed delays," *Automatica*, vol. 26, no. 5, pp. 903–908, 1990.
- [18] J. Nilsson, *Real-Time Control Systems with Delays*. Ph.D. Thesis, Lund Institute of Technology, 1998.
- [19] G. Raju, G. Verghese, and T. Sheridan, "Design issues in 2-port network models of bilateral remote teleoperation," in *Proc. IEEE Int. Conf. Robot. Automat.*, pp. 1317–1321, 1989.
- [20] B. Hannaford, "A design framework for teleoperators with kinesthetic feedback," *IEEE Trans. Robot. Automat.*, vol. 5, pp. 426–434, August 1989.
- [21] G. Leung, B. Francis, and J. Apkarian, "Bilateral controller for teleoperators with time delay via mu-synthesis," *IEEE Trans. Robot. Automat.*, vol. 11, no. 1, pp. 105–116, 1995.
- [22] H. Kazerooni, T. Tsay, and K. Hollerbach, "A controller design framework for telerobotic systems," *IEEE Trans. Contr. Syst. Technol.*, vol. 1, pp. 50–62, March 1993.
- [23] Y. Yokokohji and T. Yoshikawa, "Bilateral control of master-slave manipulators for ideal kinesthetic coupling-formulation and experiment," *IEEE Trans. Robot. Automat.*, vol. 10, pp. 605–620, October 1994.
- [24] K. Hashtrudi-zaad and S. Salcudean, "Analysis of control architectures for teleoperation systems with impedance/admittance master and slave manipulators," *Int. J. Robot. Res.*, vol. 20, no. 6, pp. 419–445, 2001.

- [25] M. Spong, "On the robust control of robot manipulators," *IEEE Tran. Automat. Cont.*, vol. 37, pp. 1782–1786, 1992.
- [26] C. Abdallah, D. Dawson, P. Dorato, and M. Jamshidi, "Survey of robust control for rigid robots," *IEEE Control Systems*, pp. 24–30, 1991.
- [27] H. Lu and W. Lin, "Robust controller with disturbance rejection for hydraulic servo systems," *IEEE Trans. Indus. Elec.*, vol. 39, pp. 157–162, February 1993.
- [28] N. Niksefat and N. Sepehri, "Robust force controller design for an electro-hydraulic actuator based on nonlinear model," in *Proc. IEEE Int. Conf. Robot. Auto.*, pp. 200–206, 1999.
- [29] N. Sadegh and R. Horowitz, "Stability and robustness analysis of a class of adaptive controllers for robotic manipulators," *Int. J. Robot. Research*, vol. 9, pp. 74–92, June 1990.
- [30] J. Colgate, "Robust impedance shaping telemanipulation," *IEEE Trans. Robot. Automat.*, vol. 9, pp. 374–384, August 1993.
- [31] Z. Hu, S. Salcudean, and P. Loewen, "Robust controller design for teleoperation systems," in *Proc. IEEE Int. Conf. Sys. Man Cyber.*, pp. 2127–2132, 1995.
- [32] S. Sirouspour, "Robust control design for cooperative teleoperation," in *Proc. IEEE Int. Conf. Robot. Automat.*, pp. 1145–1150, 2005.
- [33] J. H. Ryu, D. S. Kwon, and B. Hannaford, "Stable teleoperation with time-domain passivity control," *IEEE Trans. Robot. Automat.*, vol. 20, April 2004.

- [34] R. Jee-Hwan, K. Dong-Soo, and B. Hannaford, "Stable teleoperation with time-domain passivity control," *IEEE Trans. Robot. Automat.*, vol. 20, no. 2, pp. 365–373, 2004.
- [35] R. Kress and J. Jansen, "Automatic tuning for a teleoperated arm controller," in *Proc. Conf. on Decision and Control*, December 1992.
- [36] K. Hashtrudi-Zaad and S. Salcudean, "Adaptive transparent impedance reflecting teleoperation," in *Proc. IEEE Int. Conf. Robot. Automat.*, April 1996.
- [37] M. Shi, G. Tao, H. Liu, and J. H. Downs, "Adaptive control of teleoperation systems," in *Proc. Conf. on Decision and Control*, December 1999.
- [38] W. Zhu and S. Salcudean, "Stability guaranteed teleoperation: an adaptive motion/force control approach," *IEEE Trans. Automat. Contr.*, vol. 45, pp. 1951–1969, November 2000.
- [39] H. K. Lee, M. H. Shin, and M. J. Chung, "Adaptive control of master-slave systems for transparent teleoperation," *Journal of Robotic Systems*, vol. 15, pp. 465–475, 1998.
- [40] L. J. Love and W. J. Book, "Force reflecting teleoperation with adaptive impedance control," *IEEE Trans. Syst., Man, Cybern.*, vol. 34, no. 1, pp. 159–165, 2004.
- [41] K. Ciliz and K. S. Narendra, "Multiple model based adaptive control of robotic manipulators," in *Proc. Conf. on Decision and Control*, December 1994.
- [42] M. B. Leaby and S. J. Sablan, "Multiple model-based control of robotic manipulators: an overview," in *Proc. Conf. on Decision and Control*, December 1990.

- [43] K. S. Narendra and J. Balakrishnan, "Adaptive control using multiple models," *IEEE Trans. Automat. Contr.*, vol. 42, February 1997.
- [44] Y. Zhang and J. Jiang, "Integrated active fault-tolerant control using IMM approach," *IEEE Trans. Aerosp. Electron. Syst.*, vol. 37, October 2001.
- [45] K. Hashtrudi-Zaad and S. Salcudean, "Transparency in time-delayed systems and the effect of local force feedback for transparent teleoperation," *IEEE Trans. Robot. Automat.*, vol. 18, no. 1, pp. 108–114, 2002.
- [46] P. Arcara and C. Melchiorri, "Control schemes for teleoperation with time delay: A comparative study," *Robotics and Autonomous Systems*, vol. 38, no. 1, pp. 49–64, 2002.
- [47] S. Lee and H. Lee, "Modeling, design, and evaluation of advanced teleoperator control systems with short time delay," *IEEE Trans. Robot. Automat.*, vol. 9, no. 5, pp. 607–623, 1993.
- [48] N. Ando, J. Lee, and H. Hashimoto, "A study on influence of time delay in teleoperation," in *Proc. IEEE/ASME Int. Conf. on Advanced Intelligent Mechatronics*, September 1999.
- [49] T. Mirfakhrai and S. Payandeh, "A model for time-delays for teleoperation over the Internet," in *Proc. IEEE Int. Sym. on Computational Intelligence in Robotics and Automation*, July 2001.
- [50] J. Azorin, O. Reinoso, J. Sabater, R. Neco, and R. Aracil, "Dynamic analysis for a teleoperation system with time delay," in *Proc. IEEE Conf. on Control and Applications*, June 2003.

- [51] T. Imaida, Y. Yokokohji, T. Doi, M. Oda, and T. Yoshikawa, "Groundspace bilateral teleoperation of ets-vii robot arm by direct bilateral coupling under 7-s time delay condition," *IEEE Trans. Robot. Automat.*, vol. 20, no. 3, pp. 499–511, 2004.
- [52] R. Anderson and M. Spong, "Bilateral control of teleoperators with time delay," *IEEE Trans. Automat. Contr.*, vol. 34, no. 5, pp. 494–501, 1989.
- [53] G. Niemeyer and J.-J. Slotine, "Stable adaptive teleoperation," *IEEE J. Oceanic Eng.*, vol. 16, no. 1, pp. 152–162, 1991.
- [54] G. Niemeyer and J. Slotine, "Towards force-reflecting teleoperation over Internet," in *Proc. IEEE Int. Conf. Robot. Auto.*, pp. 1909–1915, 1998.
- [55] R. Anderson and M. Spong, "Asymptotic stability for force reflecting teleoperators with time delay," *Int. Journ. Robotics Research*, vol. 11, pp. 135–142, April 1992.
- [56] Y. Yokokohji, T. Imaida, and T. Yoshikawa, "Bilateral control with energy balance monitoring under time-varying communication delay," in *Proc. IEEE Int. Conf. Robot. Automat.*, pp. 2684–2689, 2000.
- [57] H. Baier, "Transparency and stability of bilateral kinesthetic teleoperation with time-delayed communication," *Journal of Intelligent and Robotic Systems: Theory and Applications*, vol. 40, no. 1, pp. 1–22, 2004.
- [58] G. Niemeyer and J. Slotine, "Telemanipulation with time delays," *Int. J. Robot. Research*, vol. 11, no. 2, pp. 873–890, 2004.

- [59] Y. Yokokohji, T. Imaida, and T. Yoshikawa, "Bilateral teleoperation under time-varying communication delay," in *Proc. IEEE/RSJ Int. Conf. on Intelligent Robots and Systems*, 1999.
- [60] C. Benedetti, M. Franchini, and P. Fiorini, "Stable tracking in variable time-delay teleoperation," in *Proc. IEEE/RSJ Int. Conf. on Intelligent Robots and Systems*, 2001.
- [61] T. Mirfakhrai and S. Payandeh, "A delay prediction approach for teleoperation over the internet," in *Proc. IEEE Int. Conf. Robot. Automat.*, May 2002.
- [62] J. Ueda and T. Yoshikawa, "Force-reflecting teleoperation with time delay by signal filtering," *IEEE Trans. Robot. Automat.*, vol. 20, no. 3, pp. 613–619, 2004.
- [63] J. Yan and S. Salcudean, "Teleoperation controller design using H_∞ optimization with application to motion-scaling," *IEEE Trans. Contr. Syst. Technol.*, vol. 45, pp. 244–258, May 1996.
- [64] S. Munir and W. Book, "Internet-based teleoperation using wave variables with prediction," *IEEE/ASME Transactions on Mechatronics*, vol. 7, no. 2, pp. 124–133, 2002.
- [65] S. Ganjefar, H. Momeni, F. J. Sharifi, and M. H. Beheshti, "Behavior of Smith predictor in teleoperation systems with modeling and delay time errors," in *Proc. IEEE Conf. on Control Applications*, 2003.
- [66] F. Buzan and T. Sheridan, "A model-based predictive operator aid for telemanipulators with time delay," in *Proc. IEEE Int. Conf. on Systems, Man and Cybernetics*, 1989.

- [67] A. Bemporad, "Predictive control of teleoperated constrained systems with unbounded communication delays," in *Proc. of IEEE Conf. on Decision and Control*, 1998.
- [68] A. Casavola, E. Mosca, and M. Sorbara, "Teleoperation of constrained dynamical systems over a TCP/IP local network," in *Proc. IEEE Int. Conf. Robot. Automat.*, pp. 4122–4127, 2004.
- [69] P. Prokopiou, S. Tzafestas, and W. Harwin, "Toward variable-time-delays-robust telemanipulation through master state prediction," in *Proc. IEEE/ASME Int. Conf. on Advanced Intelligent Mechatronics*, September 1999.
- [70] G. Hirzinger, J. Heindl, and K. Landzettel, "Predictive and knowledge-based telerobotic control concepts," in *Proc. IEEE Int. Conf. Robot. Auto.*, pp. 1768–1777, 1989.
- [71] J. Kikuchi, K. Takeo, and K. Kosuge, "Teleoperation system via computer network for dynamic environment," in *Proc. IEEE Int. Conf. Robot. Automat.*, pp. 3534–3539, 1998.
- [72] Z. Ping, K. Tanaka, E. Shimizu, and M. Ito, "A teleoperating system for underwater manipulator with virtual model aid," in *Proc. IEEE Int. Conf. Robot. Automat.*, pp. 882–886, 2003.
- [73] K. Gu and S. Niculescu, "Survey on recent results in the stability and control of time-delay systems," *Journal of Dynamic Systems, Measurement, and Control*, vol. 125, pp. 158–165, 2003.

- [74] J. Richard, "Time-delay systems: an overview of some recent advances and open problems," *Automatica*, vol. 39, pp. 1667–1694, 2003.
- [75] K. Watanabe, E. Nobuyama, and A. Kojima, "Recent advances in control of time delay systems - a tutorial review," in *Proc. IEEE Conf. on Decision and Control*, 1996.
- [76] V. Kharitonov, "Robust stability analysis of time delay systems: a survey," *Annual Reviews in Control*, vol. 23, pp. 185–196, 1999.
- [77] A. Olbrot, "Robustness of time-delay systems: a survey," in *Proc. IEEE Conf. on Decision and Control*, 1988.
- [78] W. Kwon and A. Pearson, "Feedback stabilization of linear systems with delayed control," *IEEE Trans. Automat. Contr.*, vol. 25, no. 2, pp. 266–269, 1980.
- [79] Z. Artstein, "Linear Systems with Delayed Controls: A Reduction," *IEEE Trans. Automat. Contr.*, pp. 869–879, August 1982.
- [80] L. Sciavicco and B. Siciliano, *Modeling and Control of Robot Manipulators, Second Edition*. Springer-Verlag, 2000.
- [81] H. Kazerooni and M. Her, "The dynamics and control of a haptic interface device," *IEEE Trans. Robot. Automat.*, vol. 10, no. 4, pp. 453–464, 1994.
- [82] Y. Bar-Shalom and X. R. Li, *Estimation and Tracking: Principles, Techniques and Software*. Artech House, Inc., 1993.

- [83] J. Lunze, *What is a Hybrid System?*, vol. 279. Modelling, Analysis and Design of Hybrid Systems; Sebastian Engell, Goran Frehse and Eckehard Schnieder (Eds.), Springer, 2002.
- [84] L. R. Rabiner, "A tutorial on hidden markov models and selected applications in speech recognition," in *Proceedings of the IEEE*, vol. 77, February 1989.
- [85] P. S. Maybeck and R. D. Stevens, "Reconfigurable flight control via multiple model adaptive control methods," in *Proc. Conf. on Decision and Control*, December 1990.
- [86] A. Shahdi and S. Sirouspour, "Multiple model control for teleoperation in unknown environments," in *Proc. of IEEE Int. Conf. Robot. Auto.*, pp. 715–720, 2005.
- [87] Y. Bar-Shalom and T. Fortmann, *Tracking and Data Association*. Academic Press INC., 1988.
- [88] C. T. Chen, *Linear System Theory and Design*. Saunders College Publishing, 1984.
- [89] G. Goodwin, S. Graebe, and M. Salgado, *Control System Design*. New Jersey: Prentice Hall, 2001.